UNIVERSITY OF CALIFORNIA,
IRVINE

Alternative Therapies in the Treatment of Port Wine Stain Birthmarks

DISSERTATION

submitted in partial satisfaction of the requirements
for the degree of

DOCTOR OF PHILOSOPHY

in Biomedical Engineering

by

Wesley Jing-Hau Moy

Dissertation Committee:
Associate Professor Bernard H. Choi, Chair
Associate Clinical Professor Kristen M. Kelly, MD
Professor and Medical Director J. Stuart Nelson, MD

2015

DEDICATION

To

Mom, Dad, Austin, Justin and Grandma

Table of Contents

List of Figures

List of Tables

Acknowledgements

I would like to thank my advisor, Dr. Bernard Choi, for his guidance and support throughout my graduate studies, for helping me learn how to be a good researcher, and providing a great research environment for me to grow in. I would like to thank the other members on my dissertation committee, Dr. Kristen Kelly, and Dr. J. Stuart Nelson, for their advice, support and mentorship.

I would also like to thank Dr. Wangcun Jia for giving me an opportunity to work at the Beckman Laser Institute and for being my first mentor during my graduate studies, and Dr. Bruce Tromberg for being a supportive mentor in all aspects of life, both from a career/professional standpoint and for looking out my best interests in my time at the Beckman Laser Institute.

I would like to specially thank all of the undergraduate researchers who worked with me during my graduate studies and made key contributions at different stages of my dissertation research. Without their help, I would not have been able to complete my research.

I would also like to thank all the members of the Microvascular Therapeutics and Imaging Lab that I have interacted with during the course of my graduate studies, especially Dr. Sean White, Dr. Bruce Yang, former students Dr. Owen Yang, and Ryan Ferraro, for their support, guidance, and friendship over the years. I would especially like to thank Ben Lertsakdadet for his tireless effort and dedication to the many research projects we have worked on together.

Finally, I would like to thank my parents and my brothers Dr. Austin Moy and Justin Moy for their love and support during my graduate school years. I have had the unique experience of not only being able to work with both of my brothers in lab, but also had the great fortune to live together with them, and it has been an experience that I will cherish and look fondly upon for the rest of my life.

Financial support was funded in part by the Arnold and Mabel Beckman Foundation, the National Institutes of Health (grant R01HD065536), the National Institutes of Health Laser Microbeam and Medical Program (LAMMP, grant P41Eb015890), and the American Society for Laser Medicine and Surgery (grant ASLMS-55289).

CURRICULUM VITAE

Wesley Jing-Hau Moy

2012-2015 Doctor of Philosophy in Biomedical Engineering
University of California, Irvine

2010-2012 Master of Science in Biomedical Engineering
University of California, Irvine

2003-2007 Bachelor of Science in Mechanical Engineering
University of California, Berkeley

PUBLICATIONS

W. Moy, J. Yakel, C. Osorio, J. Salvador, C. Hayakawa, K. Kelly, B. Choi, "Targeted narrowband intense pulsed light on cutaneous vasculature", Submitted to Laser. Surg. Med. in April, 2015

K. Kelly, W. Moy, A. Moy, B. Lertsakdadet, J. Moy, E. Nguyen, A. Nguyen, K. Osann, B. Choi, "Investigation of Talaporfin sodium-mediated photodynamic therapy alone and in combination with pulsed dye laser on cutaneous vasculature," Jour. Invest. Derm., 2014

W. Moy, S. Patel, B. Lertsakdadet, R. Arora, K. Nielsen, K. Kelly, B. Choi, "Pre-clinical in-vivo evaluation of NPe6-mediated photodynamic therapy on normal vasculature," Laser. Surg. Med., 2012

CONFERENCE PRESENTATIONS

W. Moy, A. Moy, J. Moy, B. Lertsakdadet, K. Kelly, B. Choi, "Preclinical in-vivo evaluation of combined photodynamic and photothermal therapies on normal microvasculature", UC Bioengineering Symposium, Irvine, CA, Poster Presentation (Jun 2014)

W. Moy, A. Moy, B. Lertsakdadet, J. Moy, C. Pittman, G. Ma, K. Kelly, B. Choi, "Preclinical in-vivo comparison of photodynamic therapy on normal vasculature", American Society for Laser Medicine and Surgery Annual Meeting, Phoenix, AZ, Oral Presentation (Apr 2014)

W. Moy, J. Yakel, C. Osorio, J. Salvador, C. Pittman, K. Kelly, B. Choi, "Preclinical in-vivo evaluation of vascular targeted narrow band intense pulsed light irradiation on normal vasculature", American Society for Laser Medicine and Surgery Annual Meeting, Phoenix, AZ, Oral Presentation (Apr 2014)

W. Moy, G. Ma, J. Moy, K. Kelly, B. Choi, “Preclinical in-vivo evaluation of combination photodynamic therapy and pulsed dye laser treatment on normal vasculature”, SPIE Photonics West, San Francisco, CA, Oral Presentation (Jan 2014)

W. Moy, J. Moy, B. Lertsakdadet, K. Kelly, B. Choi, “Preclinical in-vivo evaluation of combination photodynamic therapy and pulsed dye laser treatment on normal vasculature”, Montagna Symposium for Biology of the Skin, Stevenson, WA, Oral and Poster Presentation (Oct 2013)

W. Moy, A. Moy, J. Moy, B. Lertsakdadet, K. Kelly, B. Choi, “Preclinical in-vivo evaluation of combined photodynamic and photothermal therapies on normal microvasculature”, ECI Advances in Optics for Biotechnology, Medicine and Surgery XIII, Lake Tahoe, CA, Poster Presentation (Jun 2013)

W. Moy, J. Moy, B. Lertsakdadet, K. Kelly, B. Choi, “Preclinical in-vivo evaluation of combination photodynamic therapy and pulsed dye laser treatment on normal vasculature”, American Society for Laser Medicine and Surgery Annual Meeting, Boston, MA, Oral presentation (Apr 2013)

W. Moy, J. Moy, B. Lertsakdadet, K. Kelly, B. Choi, “Preclinical in-vivo evaluation of combination photodynamic therapy and pulsed dye laser treatment on normal vasculature”, SPIE Photonics West, San Francisco, CA, Oral Presentation (Jan 2013)

W. Moy, B. Lertsakdadet, R. Arora, K. Nielsen, K. Kelly, B. Choi, “Pre-clinical in-vivo evaluation of photodynamic therapy as a potential treatment for cutaneous vascular lesions”, American Society for Laser Medicine and Surgery Annual Meeting, Kissimmee, FL, Oral presentation (Apr 2012)

W. Moy, S. Patel, B. Lertsakdadet, R. Arora, K. Nielsen, K. Kelly, B. Choi, “Pre-clinical in-vivo evaluation of NPe6-mediated photodynamic therapy on normal vasculature.” SPIE Photonics West, San Francisco, CA, Oral Presentation (Jan 2012)

ABSTRACT OF THE DISSERTATION

Alternative Therapies in the treatment of Port Wine Stain Birthmarks

By

Wesley Jing-Hau Moy

Doctor of Philosophy in Biomedical Engineering

University of California, Irvine, 2015

Professor Bernard H. Choi, Chair

Roughly 400,000 children each year are born with port wine stain (PWS) birthmarks, which are skin capillary malformations characterized by a pink-reddish color that develop into purple nodules if left untreated. While PWS birthmarks can be found anywhere on the body and are typically non-life threatening, a large majority (~90%) present on the head and neck regions and can lead to complications including dental abnormalities and may be associated with capillary malformations in other organs such as the eyes (glaucoma), and brain (seizures). Due to the unsightly nature of PWS, people that have them on exposed areas of skin (face, neck, arm or leg regions) can endure immense psychological and social suffering. The current gold standard treatment for PWS in the US is laser irradiation using the pulsed dye laser (PDL). Treatment of PWS with the PDL has limited efficacy; many patients undergo 15 or more laser treatments without seeing full clearance of the PWS, demonstrating the need to investigate alternative therapies.

In my dissertation research, I investigated alternatives to PDL treatment for PWS, including photodynamic therapy (PDT), combined PDT/PDL protocols, and alternative

light based treatments. PDT has demonstrated promise towards achieving better treatment outcomes for PWS birthmarks, however, careful selection of treatment parameters is needed to avoid unwanted side effects. I performed preclinical studies of PDT using two photosensitizers, NPe6 and Hemoporfin, to better develop safe treatment parameters. I then investigated a combined PDT/PDL protocol and determined that a synergistic effect exists between the PDT and PDL protocols, illustrating that this combined approach leads to a desired treatment outcome while minimizing side effects. To better understand the PDT treatment mechanisms in skin, I also studied the depth of injury caused by NPe6-mediated PDT in preclinical models and found a direct relationship between depth of vascular injury and light dose administered. Finally, in investigating alternatives to the PDL, I studied the use of intense pulsed light (IPL) and performed a direct comparison study to the PDL. I used computational models to characterize the predicted performance of the IPL and performed experimental studies in preclinical models.

Chapter 1 - INTRODUCTION AND BACKGROUND

One out of three children born in the US is born with some type of skin lesion[1]. Birthmarks are generally considered to be discolored or raised spots found on the skin. Multiple types of birthmarks exist and can have a psychological or social impact on the way a person is perceived[2]. These include congenital nevi, (small dark or light brown patches on the skin that may be raised and have malignant potential) venous malformations, (improperly formed veins that typically present at birth and expand proportionately with the person) hemangiomas, (which either present at birth, or shortly thereafter eventually go away on their own) and capillary malformations, such as Port Wine Stain (PWS) birthmarks(1).

Roughly 400,000 children each year are born with port wine stain (PWS) birthmarks[2]. These flat vascular lesions are characterized by a pink-reddish color and if left untreated, develop into purple nodules. Clinicians use light based therapies to treat PWS birthmarks, such as the pulsed dye laser (PDL). A large majority of PWS birthmarks present on the head and neck regions (~90%) and can lead to complications or be associated with other abnormalities in areas such as the eyes and brain [3]. Histopathology of PWS skin biopsy is characterized by normal epidermis overlying abnormal plexus of dilated blood vessels located in the upper dermis[4]. In contrast, normal skin without PWS does not exhibit these large scale capillaries in this region of the skin. PWS can be found anywhere on the body and are typically non-life threatening. However, due to the unsightly nature of PWS, people that have them on exposed areas of skin (face, neck, arm or leg regions) can endure immense psychological and social suffering[5].

The current standard treatment of PWS involves the use of lasers (especially the pulsed dye laser (PDL)) or intense pulsed light (IPL) to irradiate the malformed blood vessels in combination with cooling of the skin. Cryogen spray cooling is the use of 10-50 ms spurt of tetrafluoroethane onto the skin to lower the temperature, followed by a 30-40 ms delay before light irradiation[6].

Cooling is necessary to counteract competitive absorption of the treatment light wavelengths by epidermal melanin. The short duration also allows for spatial selectivity. The pulse duration of the cryogen spurt is so short that the temperature decrease does not affect the vessels targeted by the light therapy. After cryogen cooling, a laser emits a yellow-orange light (585-595 nm range) that is strongly absorbed by hemoglobin in the ectatic blood vessels in the upper dermis[6-8]. Thrombosis and vessel damage occur as a result of the light energy being converted to heat. Treatments that occur earlier in life tend to have better outcomes (a lightening of the skin) than treatment at adult ages where the disease has progressed much further. However, even with early treatment, some patients may undergo 15 or more treatments, and not achieve complete lesion removal[9]. Another treatment outcome that is commonly observed is temporary removal of the PWS, followed by recurrence of the disease at a later time point.

A brief review of several studies utilizing the PDL to treat PWS highlights its limitations[10-12]. Unfortunately, only a small fraction of patients experience complete blanching with PDL treatment, while the vast majority do not [13, 14]. There is a critical need to develop and improve current PDL-based therapies so that they can more effectively treat patients. The five hurdles that PDL therapies must overcome are 1) PDL therapy has difficulty removing small superficial vessels, characterized by vessel diameter <20 μm[15,

16]. 2) Light absorption via melanin content in skin limits the maximum permissible radiant exposure that can be used in a safe manner[17]. 3) Light at 585-595 nm can only penetrate a certain depth into the tissue. Thus, vessels that are beyond the depth that the PDL can reach are a limiting factor [18]. 4) Optical shielding from vessels in close clusters can affect the effectiveness of the PDL. 5) Vessel size, depth, and density vary from patient to patient, and even within patient sites[19]. This reduces the effectiveness of the same PDL treatment, and can greatly affect treatment outcomes.

An alternative therapy to the PDL is photodynamic therapy (PDT). PDT requires three main components: 1) light activated reagent, or photosensitizer, 2) presence of oxygen, and 3) a light source. The general procedure of PDT involves administration, either local or systemic, of the photosensitizer followed by the subsequent irradiation of the target area with an appropriate wavelength of light, which induces the activation of the photosensitizer[20]. This activation causes a reaction with oxygen to create cytotoxic species such as singlet oxygen or free radicals[21].

PDT was first discovered in the early 1900s by a medical student named Oscar Raab, when he demonstrated that light irradiation of the drug acridine red caused a negative effect on in vitro paramecium[22]. This study was the first to observe that light activation of the drug caused a photochemical effect that produced cytotoxic effects to cells. In 1913, Dr. Freidrich Meyer-Betz became the first human case study of PDT, when he injected 200 mg of hematoporphyrin (Hp) into his own body[23]. The concept of a photosensitive period became well known after this experiment, as Dr. Meyer-Betz remained sensitive to light for a period of 2 months. Any exposure to the light in the absorption spectrum of the

photosensitizer caused an increase in swelling of his skin. In the 1960s-70s, a series of in vivo experiments showed the efficacy of PDT to treat animal tumors[24-26].

PDT is highly dependent on the light activation of the photosensitizer and creation of different reactive species, which then cause cellular damage. Wavelengths of light at the peak of the absorption spectrum cause an excitation of the molecular energy level from its ground state into a higher singlet state. The excited molecules can then: 1) return to ground state, or 2) transition to a triplet state. In the triplet state, a return back to the ground state is spin forbidden, resulting in a long excited state, where the molecules can interact with their surroundings. These two specific processes constitute the Type I and Type II reactions. Type I reactions typically involve electron or hydrogen atom transfer to non-oxygen molecules, known as reactive radicals[27]. In turn, these radicals then interact with oxygen, creating reactive oxygen species (ROS). These ROS are highly cytotoxic and induce apoptosis, or cellular death, when they come in contact with biological cells. Type II reactions utilize a direct energy transfer of the excited photosensitizer with triplet state oxygen ($^3O_2$), which then directly create singlet oxygen ($^1O_2$) [21]. Both Type I and Type II processes can occur simultaneously, but specific conditions may induce one type over the other. When hypoxic conditions and high photosensitizer concentration environments exist, Type I reactions may dominate due to the lack of oxygen present, while Type II reactions may dominate if high oxygen environments exist.

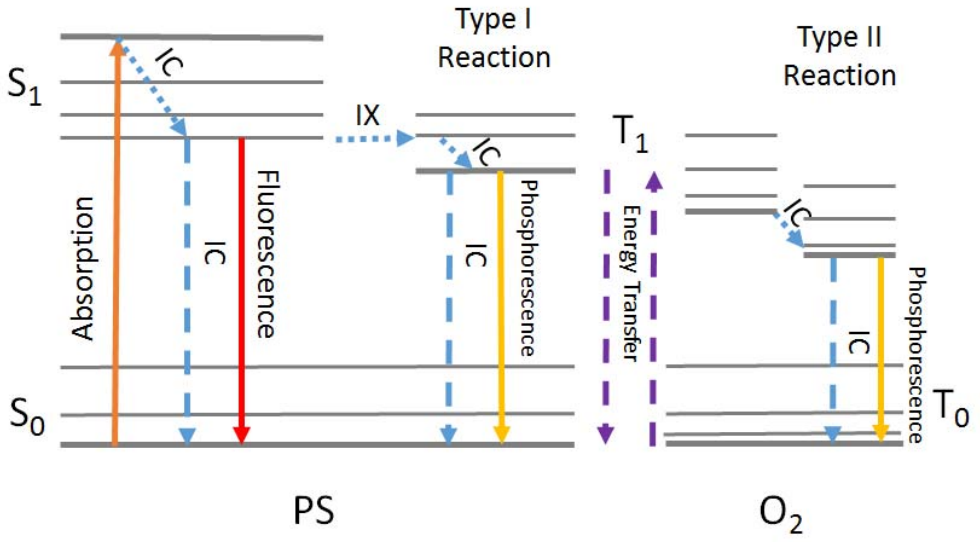

Figure 1.1 Jablonski diagram illustrating absorption of light and transition processes. PS, photosensitizer; IC, internal conversion; IX, intersystem crossing.

Any cellular structure that comes into contact with singlet oxygen or ROS can be functionally and structurally altered such that cell death is inevitable. Due to the nature of ROS and singlet oxygen (highly reactive and short lifetime), specific cellular structures can be targeted by localizing the photosensitizer. For vascular applications, this means that by limiting where the activation of the photosensitizer takes place, we can selectively target only the blood vessels, while preserving surrounding tissues. The tissue damage caused by PDT can typically be broken down into two types of mechanisms: 1) cell death directly by interaction of ROS and singlet oxygen, and 2) vascular damage and activation of the immune system.

Apoptosis and necrosis are the two general forms of cell death that occur as a result of direct PDT effects on cells. Programmed cell death (apoptosis) is a naturally occurring process that is triggered by intra- and extracellular signals. The typical response to

apoptosis is not to induce the inflammatory response, but rather the activation of macrophages that engulf the dead cells. Necrosis occurs when cells are damaged such that they are no longer viable and typically results in a pronounced inflammatory response to the region where necrotic tissue exists[28, 29]. The volume of tissue affected by necrosis and apoptosis are typically governed by the photosensitizer[29], cell type and specific light dose[30]. After a PDT treatment, necrosis and apoptosis can be clearly differentiated, with necrosis occurring at the site of photosensitizer activation, while apoptosis occurs in the boundary surrounding the necrotic area.

In blood vessels, one immediate after effect of PDT treatment is a hypoxic environment. One prevailing theory that currently exists is that vascular collapse and the consumption of the oxygen present in the blood during the PDT reaction may cause surrounding cells to become resistant to additional PDT damage[31]. Large efforts have been made to monitor tissue oxygenation and blood flow during PDT treatment[32-35], and blood flow measurements are discussed in future chapters.

Utilizing PDT to treat PWS is not a new phenomenon, and studies performed in China have demonstrated in the past decade that PDT can be effective in blanching PWS and causing permanent shutdown of flow in unwanted blood vessels. A study using blue light to activate a porphyrin derivate for the treatment of PWS resulted in observations of skin necrosis[36]. This particular study highlights the dangers of using too high of an irradiance when performing PDT to induce blanching of the PWS. A study of 238 patients using Photocarcinorin-mediated PDT, coupled with a copper vapor laser resulted in excellent results in 28% of patients, 32% reporting good results, 37% reporting fair results and a poor response in 3%, after 2-4 treatment sessions. Utilizing these forms of PDT has a

double-edged sword effect; the resulting treatment is promising in efficacy, but severe side effects included long term photosensitivity (a period up to 4 weeks where patients were required to avoid sun exposure), and a significant risk of scarring when radiant exposures were too high. This particular effect occurs when deep vascular damage results from high light doses during PDT. Deep vascular damage causes an upstream effect that compromises the structure and integrity of vessels closer to the surface of the skin, creating an ischemic necrosis effect (further investigated in chapter 6).

Our group began to develop the idea to use PDT for vascular applications by studying Porfimer Sodium-mediated PDT in 1998. Results from this study, conducted by Dr. Stuart Nelson, indicated that Porfimer Sodium-mediated PDT would be able to effectively cause PWS blanching, but that side effects including scarring, deep vascular damage, and 30+ days of photosensitivity, would preclude any type of clinical utility. To date, this study remains unpublished, however, it became the basis for future experiments to explore and characterize PDT as a potential treatment option for PWS. Our group then proceeded to investigate Benzoporphyrin Derivative Monoacid Ring A (BPD) mediated PDT in the chick chorioallantoic membrane microvascular model[37, 38]. Additionally, the new concept of combining treatment protocols of PDT and PDL was also introduced, and will be a central theme moving forward. The results of the CAM model studies demonstrated that the combined PDT+PDL protocol resulted in significantly more vascular damage than any other group. It also suggested that a synergistic interaction existed between PDT and PDL treatment protocols[38].

Our group then proceeded to conduct further preclinical animal studies to evaluate the effectiveness of BPD-mediated PDT in combination with PDL. We proceeded to utilize

the dorsal window chamber model, which will be discussed in more detail later. In the first study utilizing the dorsal window chamber model, we compared BPD PDT, PDL, and PDT+PDL[39]. One mg/kg drug dosage was administered intravenously to Sprague Dawley rats and the following interventions were evaluated: control (no drug, no light), PDT alone (16 min exposure time), PDL alone at 7 J/cm^2, PDL alone at 10 J/cm^2, PDT+PDL (PDL at 7 J/cm^2), and PDT+PDL (PDL at 10 J/cm^2). For PDT, a 576nm laser source was utilized over a 10 mm diameter spot, and for PDL, a 585nm, 1.5ms pulse duration, and 7 mm spot was utilized. Experimental observations were made at the following time points: before each treatment, immediately after, and 18 hours post intervention. No blistering, ulceration or scabbing was seen in any of the experiments. Using a blood flow monitoring technique called laser speckle imaging (LSI, which will be further discussed in more depth), reduction in blood flow was observed in all experiments, with PDT+PDL at 7 J/cm^2 resulting in the largest reduction in blood flow.

In a second follow up study[40], improvements in the surgical technique to install the dorsal window chamber enabled a longer evaluation period than the previous 18 hour time point. Our group performed the following interventions on Golden Syrian hamsters, after injection of BPD at one mg/kg drug dosage: control (no light, no drug), control (drug, no light), PDT alone (25-96 J/cm^2), PDL alone (7 J/cm^2), and PDT (25 or 75 J/cm^2) + PDL (7 J/cm^2). LSI was used to monitor blood flow dynamics and was performed before, immediately after, and at days 1, 3, and 5 post-intervention. Similar to the first study of BPD-PDT + PDL, the combined PDT+PDL protocol resulted in complete vascular shutdown sustained over the 5 day monitoring period.

Demonstrating that the combined PDT+PDL protocol was effective, our group translated these findings into a Phase I FDA approved clinical trial of PDT+PDL treatment for PWS[41]. PWS patients were recruited from a patient population with non-facial PWS. Subjects had four sites evaluated: control (no drug, no light), PDL only (585 nm, 1.5 ms pulse duration, 8 J/cm^2), PDT, and PDT+PDL. PDT was performed using a 576 nm continuous wave laser, at 6 mg/m^2 drug dosage. Our group evaluated radiant exposures of 15, 30, 45, 60, 75 and 90 J/cm^2. At PDT = 75 J/cm^2 and greater in combination with the PDL, we observed near complete blanching, indicating that the combined protocol was able to achieve improved efficacy compared to either treatment alone. We concluded from this study that the initial clinical experiments support our hypothesis that PDT+PDL can be a more effective therapy for selective removal of cutaneous microvasculature.

After investigating BPD-mediated PDT in combination with the PDL, we then focused our efforts to characterizing a new, promising photosensitizer, Mono-l-aspartyl chorlin-e6 (NPe6). NPe6 is a vascular specific photosensitizer and was selected due to its potential to cause permanent shutdown in blood vessels. The combined PDT+PDL protocol was demonstrated to achieve an enhanced vascular effect while avoiding the risks and limitations inherent to either therapy alone. By combining the two protocols, we demonstrated that lower radiant exposures could be used (chapter 3), while providing a synergistic effect to cause persistent vascular shutdown. The usage of lower light doses enables a minimization of adverse effects like scarring or skin necrosis.

In addition to NPe6, we also investigated the most commonly used photosensitizer in China for treatment of PWS, Hemoporfin (HMME). Several studies have shown that PDT (Photocarcinorin (PSD-007) and HMME) is somewhat of an effective form of treatment for

PWS[42-46], however there are several side effects including prolonged photosensitivity period (4+ weeks), the perseverance of smaller blood vessels post PDT treatment[44], secondary scar formation[47], and PDT-induced hyperpigmentation. We focus more on characterizing HMME in chapter 5.

In order to quantify the efficacy of the treatments, we utilized the dorsal window chamber model[48]. As had been used in previous studies[39, 40], the dorsal window chamber model allows for epidermal or dermal irradiation and subdermal imaging[49]. This method involves the installation of a titanium frame that provides access (i.e. window) to the skin microvasculature on the backside of a mouse. The animal is first anesthetized and its fur is removed using a depilatory cream to leave a smooth skin surface. The eyes of the animal subject were then lubricated using a sterile ophthalmic ointment to prevent drying of the cornea. The dorsal skin of the mouse is pulled taut, resulting in a front and back layer of skin. To better visualize the target vasculature, the skin was transilluminated with a white light source. One half of the window chamber frame was used as a template for proper placement of the window chamber. Using three 16 gauge needles, holes were made in the dorsal skin using the half window chamber frame template. The needles were then removed and the full titanium frame was assembled using screws and nuts through the previously made holes to secure the chamber in place. A spacer sleeve was installed over the screws (typically made of Tygon tubing), to create the proper distance between each half of the frame. Next, surgical sutures were used to keep the skin in place, and not allow for the target vasculature to be affected. After installation of the frame onto the taut skin, the front side skin flap is removed by using forceps to pinch the skin and surgical scissors, revealing the backside skin vasculature. A small border (<0.5mm) of skin around

the frame opening is left to prevent leakage of fluid from the window chamber. Microscissors and forceps are used to remove fascia from the exposure back layer skin. A glass cover slip is installed with a small injection of saline to keep the frame enclosure moist, followed by a plastic retention ring to keep everything in place. This model was used extensively to evaluate the effectiveness of each treatment protocol (PDT, PDL, combined PDT/PDL and alternative light sources).

To monitor blood flow dynamics within the window chamber, we employed the use of Laser Speckle Imaging (LSI). LSI is a useful technique as it is non-invasive and the instrumentation is simple. It was originally developed for imaging tissue vascular structures in the early 1980s[50, 51], and recent improvements to the method include use of a CCD camera and advancements to the image processing algorithms[52, 53]. The main components are a laser, a diffuser, a camera, and imaging software to process the data. LSI utilizes the speckle pattern that is formed by a laser illuminating a surface. Incident coherent light from the laser on the surface is scattered due to the inherent changes of roughness on the surface, resulting in constructive and deconstructive interference of the light. Intensity is visualized as the algebraic addition of all wave amplitudes arriving at each point, visually seen as a random distribution of areas of high intensity, when the waves add together in phase, or low to no intensity, when the individual waves are added together and cancel each other out. This speckle pattern can then be used to quantify the movement of scattering particles on the laser-illuminated surface, as the moving scattering particles induce a phase shift of the scattered light producing temporal fluctuations in the speckle pattern. From a biological tissue perspective, scattered light producing temporal

fluctuations also includes contributions from subsurface moving scatterers to the speckle pattern.

Laser speckle is a random phenomenon that can only be described statistically. An expression for the contrast of a speckle pattern was derived by Goodman et al[54], and is the basis for all LSI techniques used in our lab. There are several factors that determine the spatial and temporal characteristics of a speckle pattern. They include the size, shape, material, texture, and motion of the illuminated object, as well as wavelength, spectral bandwidth and polarization of the light source used to create the speckle pattern.

Images of time-varying speckle patterns can then be captured at set exposures times by a camera, and information about the movement of the scattering particles can be calculated. After the images are acquired, a speckle contrast image is computed. This involves the use of a sliding window algorithm (typically 7x7), where the mean (<I>) and standard deviation (σ) are computed for each pixel of interest as the sliding window progresses through the image. This computation yields a speckle contrast value (K) for each pixel of interest.

$$K = \frac{\sigma}{\langle I \rangle}$$

Computed speckle contrast values lie between 0 and 1, and the speckle size can be determined by changing the aperture stop in a camera.

When an object moves after it has been illuminated with laser light, the speckle pattern of the object will fluctuate. For small movements, on the same order magnitude as the size of the speckles, the speckle pattern will move with the object and remain correlated. In the case where the motion is much larger than the speckle size, the speckle pattern will decorrelate and change completely. Decorrelation can also occur when light is

scattered from a fluid that is constituted by a high concentration of particles. In relation to the speckle contrast, large speckle fluctuations are seen as a reduction in the contrast value when images are taken at a fixed exposure time. The amount of reduction of contrast is the basis for LSI.

Fercher and Briers originally published a paper using LSI for flow visualization using single exposure photography[51] in 1982. In this paper, they introduced a method using spatial statistics of time integrated speckle to measure blood flow in the retina. Utilizing a short exposure time on the same order magnitude as the correlation time of the intensity fluctuations, they were able to demonstrate that a high speckle contrast image could be acquired. Long exposure times would allow for the speckles to average out, resulting in a low contrast pattern. In simpler terms, high velocity equates to faster intensity fluctuations that can lead to more averaging over a set integration time. Goodman's early work on speckle resulted in the following relationship between flow velocity and contrast reduction.

$$\sigma^2(T) = \frac{1}{T}\int_0^T C_t(\tau)d\tau$$

In this equation, spatial variance of the intensity of time averaged speckles (σ^2) is a function of the autocovariance of the intensity fluctuations (C_t), and exposure time (T). With the assumption of a Lorentzian velocity distribution,

$$|C_t(\tau)| = e^{\frac{-|t|}{\tau_c}}$$

we see the following reduction of the equation:

$$\frac{\sigma}{\langle I\rangle} = \left[\frac{\tau_c}{2T}\left\{1 - e^{\frac{-2T}{\tau_c}}\right\}\right]^{\frac{1}{2}} = K$$

For all studies performed in this dissertation, we employed a simplified LSI processing algorithm. Briers et al.[55] demonstrated that the relationship between speckle contrast and correlation time can be affected depending on what velocity distribution model is used to process LSI. However, a study performed by Ramirez-San-Juan et al.[53], rederived the LSI equation utilizing a Gaussian velocity model, and demonstrated that for most practical speckle contrast values (0 to 0.6), utilizing a Lorentzian or Gaussian velocity distribution resulted in identical values for speckle contrast and correlation time. Thus, use of the simplified algorithm is justified and can be seen in the computation of Speckle Flow Index (SFI).

$$SFI = \frac{1}{2TK^2}$$

Exposure time of the image being acquired is represented by T and K is the speckle contrast value.

LSI was used to quantify blood flow dynamics over a seven day period. Figure 1.2 shows a representative example of blood flow monitoring using LSI on a dorsal window chamber model of the microvasculature.

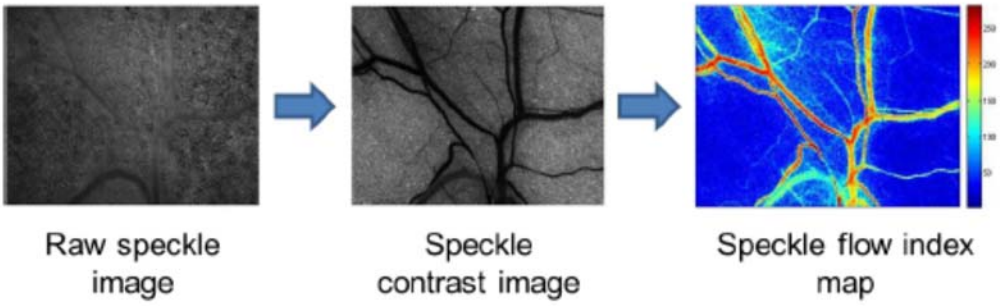

Figure 1.2 Calculation of SFI from raw speckle to speckle contrast images

To evaluate the microvascular response to each type of treatment with SFI image analysis, we adapted an iterative selection method on the data[56]. The SFI images were then categorized into a binary scale, where "1" represented complete shutdown of blood flow, and "0" represented persistent or partial blood flow. These results were then tabulated into a dose response analysis [57]. Our group has previously employed this method in several other studies[58, 59], in order to determine a characteristic radiant exposure, or a specific radiant exposure that was associated with a set probability of predetermined response.

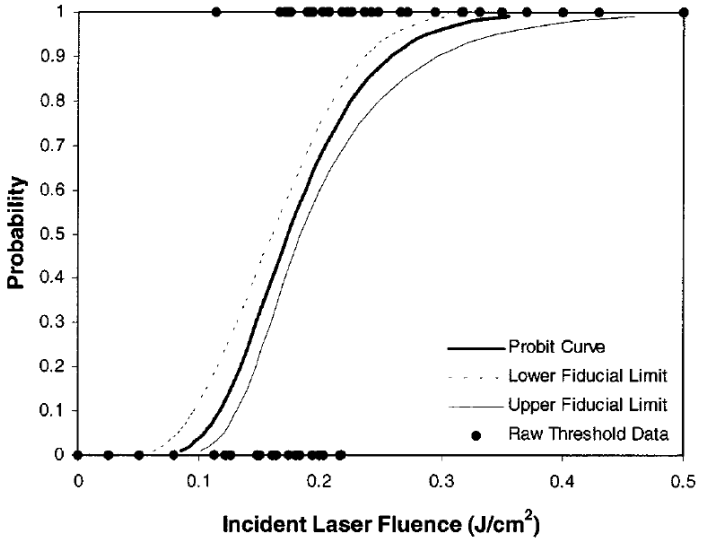

Figure 1.3 Dose response curve used to estimate the threshold radiant exposure needed for kidney stone ablation[60]. 45 individual experiments were conducted and were graded with a binary response: no audible ablation event ("0") and audible ablation event ("1").

The above figure is used to determine the energies needed for successful kidney stone ablation. We utilized the same approach, changing the axes to fit our criteria of persistent vascular shutdown (y-axis) and radiant exposures needed to cause this effect (x-axis). After utilizing this analysis, we were able to then identify sub-therapeutic regions below the characteristic radiant exposures calculated from the dose response analysis

performed on each study. This led to the rationale of combining PDT and PDL treatment protocols to evaluate if there was an additive or synergistic effect. By using radiant exposures determined to be sub-therapeutic when only performing one treatment protocol but combining them together, we then evaluated the effectiveness over a large set of treatment parameters (chapter 3).

Chapter 2 - PRECLINICAL IN VIVO EVALUATION OF NPE6-MEDIATED PHOTODYNAMIC THERAPY ON NORMAL VASCULATURE

We report our initial study of NPe6-mediated photodynamic therapy within a rodent dorsal window chamber model based on laser speckle imaging (LSI) and dose response analysis. We demonstrate that NPe6-mediated PDT can cause persistent vascular shutdown within the blood vessels in the animal model and can be a possible treatment protocol for port wine stain disease.

Abstract

Current treatments of port-wine stain birthmarks typically involve use of a pulsed dye laser (PDL) combined with cooling of the skin. Currently, PDL therapy protocols result in varied success, as some patients experience complete blanching, while others do not. Over the past decade, we have studied the use of photodynamic therapy (PDT) as either a replacement or adjuvant treatment option to photocoagulate both small and large vasculature. The objective of the current study was to evaluate a PDT protocol that involves use of an alternate intravascular photosensitizer mono-Laspartylchlorin-e6 (NPe6) activated by an array of low cost light emitting diodes.

To monitor the microvasculature, a dorsal window chamber model was installed on 22 adult male mice. The light source consisted of a custom-built LED array that emitted 10 W at a center wavelength of 664 nm (FWHM ± 20 nm). The light source was positioned at a fixed distance from the window chamber to achieve a fixed irradiance of 127 mW/cm^2. A retroorbital injection of NPe6 (5 mg/kg) was performed to deliver the drug into the

bloodstream. Laser irradiation was initiated immediately after injection. To monitor blood-flow dynamics in response to PDT, we used laser speckle imaging. We employed a dose–response experimental design to evaluate the efficacy of NPe6- mediated PDT.

We observed three general hemodynamic responses to PDT: (1) At low radiant exposures, we did not observe any persistent vascular shutdown; (2) at intermediate radiant exposures, we observed an acute decrease in blood flow followed by gradual restoration of blood flow over the 7-day monitoring period; and (3) at high radiant exposures, we observed acute vascular shutdown that persisted during the entire 7-day monitoring period. Dose–response analysis enabled identification of 85 J/cm^2 as a characteristic radiant exposure required to achieve persistent vascular shutdown at Day 7 following PDT.

The experimental data suggest that NPe6-mediated PDT can achieve persistent vascular shutdown of normal microvasculature.

2.1 Introduction

Port wine stain (PWS) is a congenital vascular malformation commonly found on the face and neck regions. Current treatments typically involve use of a pulsed dye laser (PDL) combined with cooling of the skin[9]. Yellow light, in the 585–595 nm wavelength range, is strongly absorbed by hemoglobin and can photocoagulate the targeted vasculature. Currently, PDL therapy protocols result in varied success, as some patients experience complete blanching, while others do not[61]. Many factors contribute to less than optimal PWS blanching, including reperfusion, angiogenesis, small-diameter vessels (<20 μm) that are resistant to conventional PDL-based protocols, vascular density and depth. The limited

efficacy of PDL treatments has led us to believe that a new protocol is needed to tackle the problem of PDL-resistant small vasculature.

Over the past decade, we have studied the use of photodynamic therapy (PDT) as either a replacement or adjuvant treatment option to photocoagulate both small and large vasculature[39-41]. We previously used Benzoporphyrin Derivative Monoacid Ring A (BPD) as the photosensitizer, and studied treatment protocols involving PDT alone, PDL alone or the combination of photodynamic and PDL therapies. Our preliminary preclinical and clinical data suggest that the combination protocol is a superior method to induce persistent shutdown of the vasculature. Unfortunately, our implementation of BPD-mediated PDT is limited due to the high cost of BPD and the lack of availability of 576-nm light sources.

In our current study, we devised a protocol that involves use of an alternate intravascular photosensitizer mono-L-aspartylchlorin-e6 (NPe6) activated by an array of low-cost light emitting diodes (wavelength = 664 ± 20 nm)[62]. Previous studies have demonstrated that NPe6 is an effective photosensitizer for mediating light induced changes to the microvasculature[63, 64]. To assess therapeutic efficacy, we used the mouse dorsal window chamber model and laser speckle imaging to monitor blood- flow dynamics. In multiple published studies[39, 40, 48, 65-68], we have used this combination to monitor the hemodynamic response of the vasculature to phototherapeutic protocols.

2.2 Materials and Methods

2.2.1 Rodent Dorsal Window Chamber Model

To monitor the microvasculature, a dorsal window chamber model was used[48]. Twenty-two adult male mice (25–30 g, C3H strain) were used in accordance with a protocol approved by the Institutional Animal Care and Use Committee at University of California, Irvine. The window chamber model was prepared for convenient, longitudinal observation of the vascular network on the subdermal side of the mouse, and is described in detail by Moy et al[48]. Animals were anesthetized with a combination of ketamine and xylazine (2:1 ratio, 0.1/100 g body weight) administered through intraperitoneal injection. Two titanium window chamber frames were implanted on the back of each animal using screws, spacers, and nuts. Sutures were used to restrict movement of the skin within the chamber, preserving the location of the vasculature over the 7-day evaluation period. A full thickness of skin was removed, revealing the subdermal layer of vasculature. To prevent dehydration, isotonic saline solution was applied onto the exposed skin, followed by placement of a glass cover slip and retention ring to hold the solution in place. The animal was allowed to recover for ~24 hours prior to PDT.

2.2.2 Light Source

The light source consisted of a custom-built LED array, provided by Light Sciences Oncology, that emitted 10 W at a center wavelength of 664 nm (FWHM ± 20 nm). Light output was controlled with a variable-current power supply. PDT Protocol To perform PDT, a custom light-tight box was developed. The animal was anesthetized with isoflurane (5%) delivered with a nose cone placed over its snout. An aperture was used to isolate the window chamber and avoid irradiation of surrounding tissue regions. The light source was

positioned at a fixed distance from the window chamber to achieve a fixed irradiance of 127 mW/cm^2. The irradiation time was varied as described below. NPe6 was reconstituted using 4 ml of double deionized water in a 10 ml vial, to create a stock solution of 25 mg/ml. A retroorbital injection of NPe6 (5 mg/kg) was performed to deliver the drug into the bloodstream. Laser irradiation was initiated immediately after injection.

2.2.3 Laser Speckle Imaging (LSI)

To monitor blood-flow dynamics in response to PDT, we used laser speckle imaging (LSI). The imaging instrument was nearly identical to that described by Bui et al[65]. Briefly, the animal was anesthetized with isoflurane (5%) delivered with a nose cone placed over its snout. The animal was positioned with the subdermal side of the window chamber imaged directly by a camera (Nuance, Caliper Life Sciences, Hopkinton, MA) equipped with a 5x zoom lens. A HeNe laser (λ = 633 nm, 30 mW) was used to irradiate the epidermal side of the window chamber and the transmitted speckle pattern imaged with the camera. A beam expander and ground-glass diffuser was used to homogenize the incident laser beam. An image exposure time of T = 10 milliseconds was used to achieve a linear response range of the instrument for the expected blood- flow speeds in the arterioles and venules. Custom software written in LabVIEW (Version 8.6, National Instruments, Austin, TX) and MATLAB (The Mathworks, Natick, MA) was used to acquire and process images.

We collected LSI data on Days 0 (i.e., day on which PDT was performed), 1, 2, 3, and 7. On Day 0, LSI data were collected immediately prior to and after PDT was completed. For each time point, a sequence of 10 raw speckle images was collected. Each image was converted to a speckle contrast image using a 7x7 sliding window. At each window

position, the mean intensity (<I>) and standard deviation (σ) were computed, and the speckle contrast (K) of the center pixel in the window was calculated using the following expression:

$$K = \frac{\sigma}{< I >}$$

A simplified speckle imaging equation[53] was used to convert each speckle contrast image to a speckle flow index (SFI) image. The equation is $SFI = (2TK^2)^{-1}$, where SFI is the reciprocal of the speckle decorrelation time.

2.2.4 Dose–Response Experimental Design

We set out to determine if NPe6-mediated PDT is capable of achieving persistent vascular shutdown and to estimate a characteristic radiant exposure required to achieve shutdown. To this end we employed a dose– response experimental design, typically used in pharmaceutical studies and also used previously in laser-tissue interaction studies[60, 69, 70]. Our independent variable was radiant exposure (0–1,000 J/cm^2), which we varied in a logarithmic fashion. Since irradiance was fixed at 127 mW/cm^2, we essentially varied the irradiation time to control radiant exposure. A single experiment was performed at each of the 20 radiant exposures, in addition to two control experiments. Additional negative control experiments were performed using either (a) the maximum radiant exposure (1,000 J/cm^2) without any NPe6 administered, or (b) the minimum radiant exposure (0 J/cm^2) with NPe6 administered.

Using Prism software (Version 5.0d, GraphPad Software, San Diego, CA), we performed a dose–response analysis to determine the RE50/7, defined as the characteristic radiant exposure at which complete vascular shutdown was achieved through Day 7.

Complete vascular shutdown was defined as no flow seen in the SFI image on Day 7, when compared to the baseline SFI image on Day 0, pre-NPe6-mediated PDT. We also determined the 95% confidence interval of the RE50/7 value.

Two authors (W.J.M. and B.C.) independently reviewed the SFI images from each of the 22 experiments and graded each one as either a ‘‘0’’ (lack of complete vascular shutdown at Day 7) or a ‘‘1’’ (complete vascular shutdown at Day 7).

2.3 Results

With LSI and the dorsal window chamber, we observed three general hemodynamic responses to PDT (Fig. 1). At low radiant exposures, we did not observe any or persistent vascular shutdown (Fig. 1A). The 0 J/cm^2 radiant energy exposure and the two control experiments exhibited this pattern, as was expected. At intermediate radiant exposures, we observed an acute decrease in blood flow followed by gradual restoration of blood flow over the 7-day monitoring period (Fig. 1B). At high radiant exposures, we observed acute vascular shutdown that persisted during the entire 7-day monitoring period.

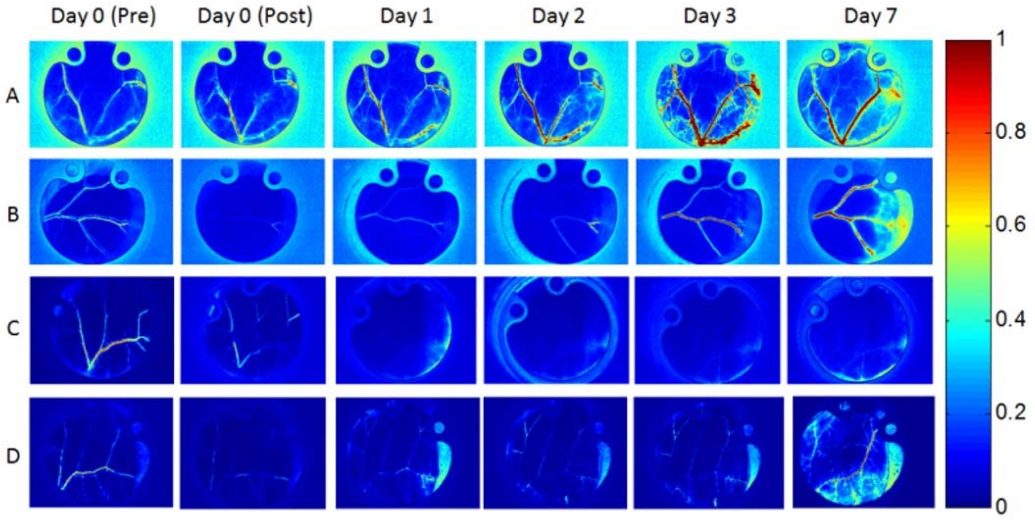

Figure 2.1 Representative SFI images of the microvasculature following irradiation. (A) No acute shutdown, no persistent shutdown on Day 7. Experiment: 0 J/cm^2 radiant exposure. (B) Acute shutdown post experiment, but no persistent shutdown on Day 7. Experiment: 60 J/cm^2 radiant exposure. (C) Acute shutdown and followed by persistent shutdown. Experiment: 700 J/cm^2 radiant exposure. For each experiment, the SFI values for each image was normalized with respect to the Day 0 (Pre) baseline.

Following the graded system explained above, we determined that 9 out of the 20 experimental conditions produced a ‘‘0’’ result, with the remaining 11 experiments producing a ‘‘1’’ result at Day 7. Radiant exposures of 80 and 100–1,000 J/cm^2 produced a ‘‘1’’ result, while radiant exposures of 0–70 and 90 J/cm^2 resulted in a ‘‘0’’. Additional negative control experiments were conducted using either (a) retroorbital administration of NPe6 and no light, or (b) no NPe6 administration and a radiant exposure of 1,000 J/cm^2. Both of these experiments resulted in a lack of acute or persistent vascular shutdown. Dose–response analysis enabled identification of 85 J/cm^2 as the RE50/7 value for NPe6, to achieve persistent vascular shutdown at Day 7 following PDT (Fig. 2.1). A fairly sharp demarcation between a ‘‘0’’ response and a ‘‘1’’ response existed, resulting in a fairly narrow 95% confidence interval of 72–95 J/cm^2 for the RE50/7 value.

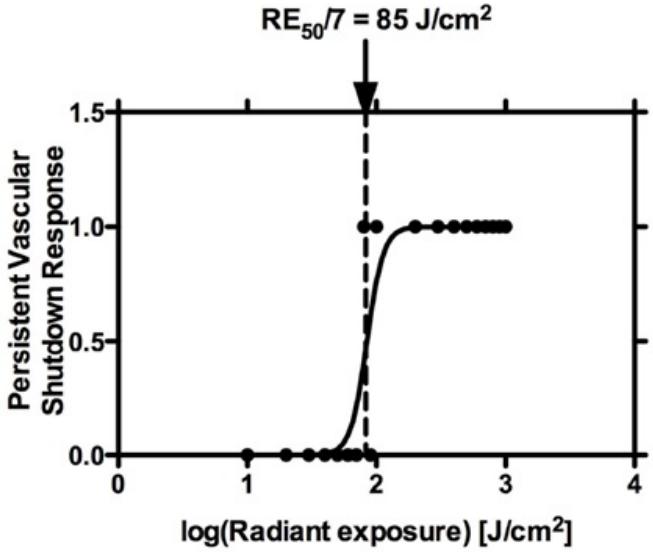

Figure 2.2 Dose-response analysis of persistent vascular shutdown response at specific radiant exposures. $RE_{50}/7$ of 85 J/cm^2 was determined from the data.

2.4 Discussion

The experimental data (Figs. 2.1 and 2.2) of this study suggest that NPe6-mediated PDT can achieve persistent vascular shutdown at doses greater than 90 J/cm^2. Given this observed efficacy of NPe6-mediated PDT, we propose that this approach is a potential treatment for PWS and other cutaneous vascular lesions in humans, and further preclinical evaluation is warranted.

Examination of SFI data from high radiant exposures (>90 J/cm^2) revealed the desired outcome of persistent vascular shutdown continuing through Day 7. The shutdown was very apparent from inspection of the SFI images, as both small and large diameter vessels showed a complete absence of blood flow. Hence, NPe6-mediated PDT can achieve shutdown of smaller-diameter vessels that otherwise may be resistant to PDL therapy.
In our previous studies involving BPD-mediated PDT, we found that persistent vascular shutdown was achieved during a 16 minutes irradiation time. During our clinical study, we

found that patient acceptance of this irradiation time was not an issue. In our current study, we determined a $RE_{50}/7$ value (85 J/cm^2) associated with an irradiation time of 10 minutes. Hence, we expect that NPe6-mediated PDT also would be tolerated by patients, at least from a time perspective. Additionally, the low cost of the LED-based light source components is expected to make the treatment more accessible and easier to adopt in the clinic.

At low radiant exposures (<80 J/cm^2) we observed an acute reduction in blood flow that gradually returned by Day 7 (Fig. 1B). These data suggest the onset of three biological response mechanisms: (a) restoration of the vascular network by reperfusion of incompletely photocoagulated microvasculature, (b) development of new blood vessels separate from existing vasculature, and (c) angiogenesis and its regenerative effects on existing vasculature. Our results of reperfusion following PDT with low radiant exposures are consistent with those from previous pulsed-laser studies that have demonstrated the difficulty of achieving persistent vascular shutdown. Our current study and these previous studies collectively demonstrate the critical need to perform longitudinal monitoring of blood flow in response to phototherapies, since immediate vascular responses (<24 hours) may differ greatly from those observed several days past the therapeutic intervention.

Our past work with BPD demonstrates that translation of PDT results from rodents to humans requires additional considerations. Light doses required for the clinical response in humans were different. In addition, we frequently observed ulceration in the rodent window model due to lack of deep vasculature (a result of the surgery) that did not occur in the human studies. Thus, the primary value of the preliminary animal experiments

is to confirm that persistent vascular shut down can be achieved; however, dosing information and side effect profiles must be determined in future clinical experiments.

Current literature does include some information about dosing and side effect profiles that will be useful for our planned clinical experiments. With respect to the safety concerns in humans of NPe6-mediated PDT, we refer to the study conducted by Chan et al[58] in which NPe6 was administered to 14 patients with basal cell carcinoma, squamous cell carcinoma or papillary carcinoma. Patients received varying drug dosages (0.5–3.5 mg/kg) and light dosages (argon pumped dye laser at 664 nm; 25–200 J/cm^2; 50–400 mW/cm^2). Ninety percent of the patients exhibited a complete response, which was defined as no clinical or histopathological evidence of tumor remaining after PDT treatment. Adverse effects were pain at the treatment site (two patients) and erythema and edema of the treatment site (one patient). Three patients experienced pruritus, facial edema, erythema, and tingling, all of which were not clearly related to treatment. Photosensitivity tested with a solar stimulator was not evident 1 week post-treatment in 12/14 subjects. One patient had erythema with the solar simulator until 3 weeks post-treatment and one patient was not tested. In Usuda et al[71], 29 patients with 38 lesions of centrally located early lung cancer received PDT with a 40 mg/m^2 dosage of NPe6, followed by 664 nm wavelength light (100 J/cm^2; 150 mW/cm^2). They achieved complete remission in 35/38 lesions (92.1%). Recurrence occurred in seven lesions. Patients were told to avoid light for 2 weeks post-treatment. The study did not report any indications of extensive necrotic damage of the tumors and no other adverse effects were noted by the authors.

Previous studies of NPe6-mediated PDT have demonstrated promising outcomes for tumor treatment[58, 62-64, 71, 72]. Our current study of NPe6-mediated PDT treatment

highlights the potential role of this therapy in treatment plans targeting unwanted cutaneous vasculature. Our future work will study the role of additional independent variables (irradiance, drug dosage, fractionation, combination protocols, etc.) on our ability to achieve persistent vascular shutdown.

2.5 Acknowledgments

The work was supported in part by grants obtained from the National Institutes of Health (HD065536), the National Institutes of Health Laser Microbeam and Medical Program (LAMMP, a P41 Biotechnology Resource, project number RR001192), and the Arnold and Mabel Beckman Foundation. The authors thank Liz Bromley and Steven Daly of Light Sciences Oncology for their generosity in providing us with NPe6 and the light source. The authors thank Dr. Tom Foster (University of Rochester) for discussions involving NPe6-mediated PDT; and Sean White and Austin Moy (both at University of California, Irvine) for assistance in preparing this manuscript.

Chapter 3 - INVESTIGATION OF TALAPORFIN SODIUM-MEDIATED PHOTODYNAMIC THERAPY ALONE AND IN COMBINATION WITH PULSED DYE LASER ON CUTANEOUS VASCULATURE

We report our second study of NPe6-mediated photodynamic therapy in combination with the pulsed dye laser (PDL). We utilized the rodent dorsal window chamber model and performed blood flow monitoring using laser speckle imaging (LSI). Pharmacokinetics of the photosensitizer was studied using fluorescence microscopy and speckle flow index (SFI) maps of the data were tabulated using dose response analysis. We demonstrate that low dose NPe6-mediated PDT in conjunction with low dose PDL can cause persistent vascular shutdown within the blood vessels in the animal model and can be a possible treatment protocol for port wine stain disease.

Abstract

Laser therapy is the standard treatment of port wine stains in the United States, but complete removal is infrequently achieved. Photodynamic therapy (PDT) is an alternative treatment option. Our previous data suggest that PDT followed immediately by pulsed dye laser (PDL) irradiation allows use of lower radiant exposures for each treatment component, achieves prolonged vascular removal, and potentially avoids risks and limitations inherent to either therapy alone. Our study objectives were to 1) establish a characteristic radiant exposure to achieve persistent vascular shutdown with PDL irradiation, 2) determine if the combined PDT+PDL approach reduces PDT radiant exposure required to achieve persistent vascular shutdown, and 3) measure the

pharmacokinetics of Talaporfin sodium to study the mechanism of action associated with this phototherapy. We estimated a characteristic radiant exposure value of 7.1 J/cm^2 with PDL irradiation. With PDT+PDL, the characteristic PDT radiant exposure required to achieve persistent vascular shutdown decreased significantly from 85 to 45 J/cm^2 ($p=0.0002$). We estimated a characteristic intravascular time for Talaporfin sodium of ~22 min. PDT+PDL achieved persistent vascular shutdown at lower radiant exposures than either treatment alone, demonstrating the potential to achieve safer and enhanced removal of cutaneous vascular lesions.

3.1 Introduction

Port wine stain (PWS) birthmarks are vascular malformations characterized by an increase in the number of blood vessels, ectasia, and dilation. Lesions are initially flat and red to pink in color. Untreated PWS birthmarks will darken to red-purple and tissue hypertrophy and nodularity may develop. The progressive disfiguration is associated with complications include bleeding, dental abnormalities, and psychosocial distress[73].

Currently, the standard treatment for PWS in the United States involves use of lasers or intense pulsed light to photocoagulate selectively the abnormal vasculature. Clinicians typically use pulsed dye lasers (PDLs, λ = 585-595 nm) and Alexandrite lasers (λ = 755 nm) to target the optical absorbers oxyhemoglobin and deoxyhemoglobin in the vessels[8, 73]. The absorbers convert the optical energy to heat, resulting in thermal damage and thrombosis in the targeted vessels[74]. With photothermal therapy, PWS often become lighter in color, but patients must undergo many treatments (15-20 are not uncommon; [75]). Furthermore, treatment of skin types IV-VI is difficult due to absorption of light by

overlying epidermal melanin, limiting both the maximum safe radiant exposure and treatment efficacy.

Photodynamic therapy (PDT) of PWS birthmarks is an alternative treatment option. PDT involves optical excitation of an exogenous photosensitizer and subsequent energy transfer from the photosensitizer to oxygen to create cytotoxic singlet oxygen (Gorman et al, 2006). Excitation of intravascular photosensitizers enables targeted destruction of the vasculature. To date, clinicians in China have the most extensive experience applying PDT to treat PWS birthmarks. In 2010, Lu et al[43] published data collected from 75 patients treated with PDT using Photocarcinorin (PSD-007) and a copper vapor laser (λ = 510.6 and 578.2 nm). They reported complete blanching of the PWS in 57% of subjects, after four or fewer treatments. Treated subjects needed to avoid sun exposure for two weeks and wore dark glasses for one month. The current state of PDT for treatment of cutaneous microvasculature is that the treatment can be effective but is associated with prolonged photosensitivity and a substantial risk of scarring.

We developed a combined PDT+PDL protocol to achieve an enhanced vascular effect while avoiding the risks and limitations inherent to either therapy alone. By combining the photochemical and photothermal aspects of PDT and PDL, we postulate that lower radiant exposures can be used for both PDT and ensuing PDL therapy, minimizing adverse effects and achieving excellent and perhaps enhanced treatment efficacy compared to either treatment alone.

We previously investigated Benzoporphyrin Derivative Monoacid Ring A (BPD) as a photosensitizer for vascular-selective PDT+PDL[39-41]. We selected BPD due to its ability to enable vascular-specific PDT and a good safety record when utilized for treatment of

macular degeneration[76]. Furthermore, we selected BPD over the porphyrin derivatives used in China, due primarily to a shorter reported period of photosensitivity (five days as opposed to several weeks;[77]). In a preclinical study, we compared BPD-mediated PDT, PDL, and combined PDT+PDL treatment protocols[40] and observed that only PDT+PDL resulted in persistent vascular shutdown sustained over the five-day monitoring period.

Based on this outcome, we then conducted a preliminary clinical study evaluating PDT+PDL versus either PDT or PDL alone[41]. We did not observe any serious adverse events and epidermal changes were mild and self-limited. We did observe an increase in the degree of blanching of the PWS birthmark associated with PDT+PDL treatment, but we unfortunately did not achieve the desired degree of blanching.

To enhance treatment efficacy, we considered alternative PDT protocols. We proposed use of Talaporfin sodium (TS; Light Science Oncology, Bellevue, Washington) as the photosensitizer. Researchers previously investigated TS for the treatment of benign prostatic hypertrophy, endobronchial cancer, hepatocellular carcinoma, gliomas, esophageal cancer, refractory solid tumors, lung cancer, and metastatic colon cancer[78-82]. TS is a promising photosensitizer for PWS treatment based on the following characteristics: 1) evidence of sufficiently-long intravascular dwell times[62]; 2) evidence of safety and tolerability in humans[78-83]; 3) relatively short photosensitivity period of approximately one week at proposed drug doses[83]; and 4) absorption at a longer wavelength (664 nm), which we postulate will enable photocoagulation of both superficial and deep vessels, depending on irradiation time.

Based on data from a preclinical study involving a rooster comb model, Ohshiro et al[84] reported that TS-mediated PDT is a promising treatment option for cutaneous

vascular lesions. In an independently-designed preclinical study involving the dorsal window chamber model[85], we established a characteristic radiant exposure of 85 J/cm^2 associated with persistent vascular shutdown following TS-mediated PDT.

The objectives of the current study were to 1) establish a characteristic radiant exposure to achieve persistent vascular shutdown with PDL irradiation, 2) determine if the combined PDT+PDL therapy reduces the PDT light dose required to achieve persistent vascular shutdown, and 3) measure the pharmacokinetics of TS in the window chamber model to study the mechanism of action associated with TS-mediated PDT and PDT+PDL protocol.

3.2 Materials and Methods

3.2.1 Dorsal window chamber model

Similar to previous work from our group[85], we performed experiments on adult C3H mice (25 to 30 g mass, n = 38). Our institutional Investigational Animal Care and Use Committee approved all experiments. We installed dorsal window chambers on each subject. We provide details of the surgical procedure in a previous publication[48].

3.2.2 Light sources and Photosensitizer

We used two light sources in this study. For PDL irradiation, we used a clinical 595-nm laser (Vbeam Perfecta, Candela Corporation, Wayland, MA). We held the following parameters constant: spot size of 10 mm diameter, pulse duration of 1.5 ms. Although clinicians typically use cryogen spray cooling with this PDL during treatment of PWS birthmarks, we found that spray cooling of the suspended window chamber led to marked deformation of the skin. For PDT, we utilized a custom-built light emitting diode array

centered at 664-nm excitation (spectral range of 20 nm). We used reconstituted TS (Light Sciences Oncology; Bellevue, Washington) into a stock solution of 25 mg/mL.

3.3.4 Treatment protocols

PDT: We used the same protocol described previously by Moy et al[85]. A 5% isoflurane was initially used to anesthetize the subject. We then moved the subject to a custom-built PDT station. During PDT, we maintained the subject under anesthesia with 1.5% isoflurane. We positioned the epidermal side of the window chamber so that it served as the irradiated surface and positioned an aperture over the window chamber to avoid stray-light irradiation of other parts of the body. We first injected TS (5 mg/kg) into the bloodstream via retro-orbital injection and began PDT immediately afterwards for the desired period of time. For all experiments, we used an irradiance of 100 mW/cm^2 and varied the irradiation time to achieve specific values of radiant exposure, ranging from 0 to 260 J/cm^2. To avoid systematic errors, we randomized the order of experiments.

PDL: We anesthetized and positioned the animal as described for the PDT protocol. We then irradiated the window chamber with a single 595-nm laser pulse. We used radiant exposures between 3.25 and 10.00 J/cm^2.

Combined PDT+PDL protocol: We performed the PDT and PDL protocols as described above. To test the hypothesis that the PDT+PDL protocol enables persistent vascular shutdown with lower radiant exposures of either PDT or PDL irradiation, we restricted our study to values of PDT (20 to 60 J/cm^2) and PDL (4 to 6 J/cm^2) radiant exposures that were below the associated $RE_{50}/7$ values for either protocol alone. We performed PDL irradiation within 5 s after PDT was complete.

3.3.5 Laser Speckle Imaging (LSI)

To monitor blood-flow dynamics associated with phototherapy, we used LSI. We described previously the specifics of LSI methodology with the window chamber[48]. While imaging the dermal side of the window chamber, we collected raw speckle image sequences generated by using transmitted 633-nm Helium-Neon laser and processed these images to Speckle Flow Index (SFI) images using a simplified speckle imaging equation[53].

3.3.6 Experimental design

In this study, we used dose-response analysis in a similar fashion to the approach described in a previous publication[85]. We performed 19 experiments to establish a dose-response curve for PDL irradiation, and 19 experiments for PDT+PDL irradiation. Based on the need for longitudinal monitoring to properly assess the fate of microvasculature after phototherapy[40], we collected raw speckle images at the following time points: before phototherapy; immediately after phototherapy; and at Days 1, 2, 3, and 7 after phototherapy. Five of the authors (BC, WJM, KMK, BSL, and JJM) independently reviewed the SFI images collected on Day 7 of each experiment and graded each set of images as either "0" (no persistent vascular shutdown on Day 7) or "1" (persistent vascular shutdown achieved on Day 7). We then used the software package Prism (version 5.0d, GraphPad Software, San Diego, CA) to fit a sigmoid to the data and estimated a characteristic radiant exposure ($RE_{50}/7$) at which persistent vascular shutdown was achieved.

3.3.7 Statistical analysis

We used an F test to compare the $\log(RE_{50}/7)$ values determined from PDT (85 J/cm^2,[85]) and from the combined PDT+PDL experimental study. We used Prism software

to perform this analysis. Our null hypothesis was that the $RE_{50}/7$ values for the two studies do not differ in a statistically significant manner.

3.3.8 Pharmacokinetic modeling

We used intravital fluorescence microscopy to collect images of the microcirculation in the window chamber after retroorbital injection of TS (1 mg/kg). We used 633-nm Helium-Neon laser light as the excitation source and collected emission light with a 4x objective and a bandpass filter (680-nm center wavelength) to isolate the TS fluorescence. We used an EMCCD camera (QuantEM:512C, Photometrics) to collect the fluorescence emission images. We first collected background fluorescence images prior to TS, administered TS to the vasculature, and collected and analyzed a time sequence of fluorescence images. We subtracted a mean background image from each post-injection image and calculated the mean fluorescence emission from specific regions of interest selected from individual blood vessels. For each region of interest, we normalized the emission at each time point to the maximum emission value. Similar to previously published studies[86, 87], we then fit a biexponential relationship to our collective data of fluorescence emission versus time from 11 regions of interest:

$$C(t) = \alpha e^{-\beta t_1} + \gamma e^{-\delta t_2}$$

Where C(t) is the fluorescence emission versus time and α, β, γ, and δ are fitting parameters. $t_1 = \ln 2/\beta$ and $t_2 = \ln 2/\gamma$ represent characteristic pharmacokinetic times. We specifically are interested in τ1, which is a characteristic intravascular time prior to significant diffusion of TS into the perivascular space.

3.3 Results

3.3.1 Dose-response analysis of data collected with 595-nm PDL irradiation

To assess blood-flow dynamics in response to PDL irradiation (10-mm spot diameter, 1.5-ms pulse duration), we collected raw speckle images at various time points before and after PDL irradiation (Figure 3.1). Similar to trends we observed previously[85], we observed three general trends: 1) minimal acute change in blood flow and no persistent vascular shutdown (Figure 3.1A); 2) marked acute change in blood flow, followed by partial to full recovery of blood flow and no persistent vascular shutdown (Figure 3.1B); and 3) marked acute or delayed reduction in blood flow, followed by complete vascular shutdown at Day 7 (Figure 3.1C). With application of dose-response methodology, we estimated a characteristic radiant exposure ($RE_{50}/7$) of 7.1 J/cm2 required to induce persistent vascular shutdown with PDL irradiation (Figure 3.1D).

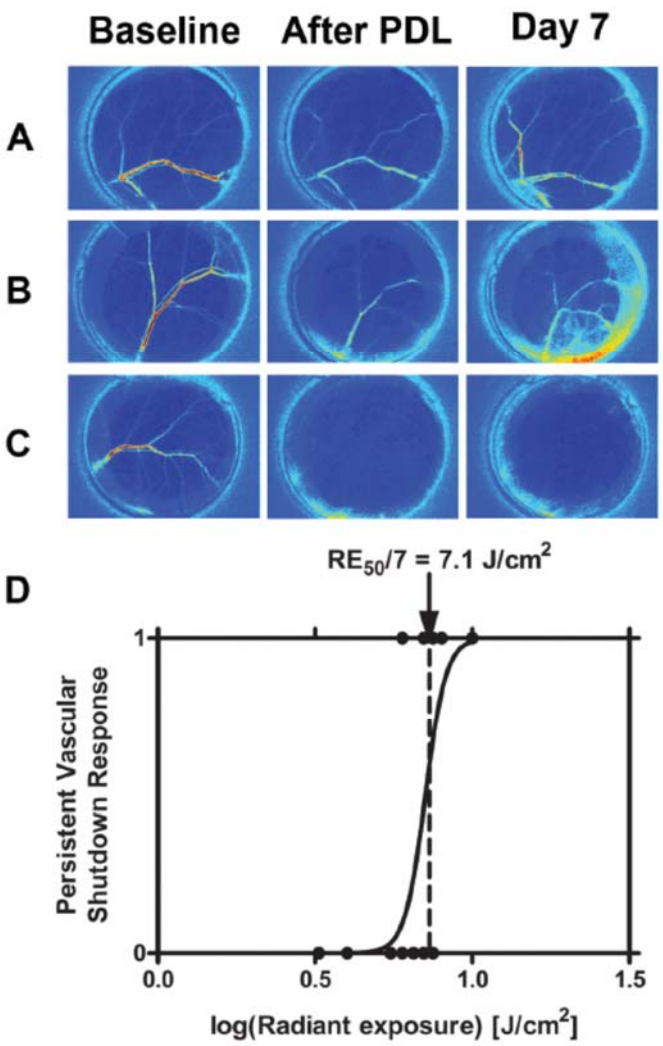

Figure 3.1 Characteristic radiant exposures associated with persistent vascular shutdown following 595-nm PDL irradiation. We performed PDL irradiation on the epidermal side of window chambers and imaged blood-flow dynamics using LSI. We assessed persistent vascular shutdown on Day 7. We assigned a "0" score to window chambers in which some evidence of blood flow was present, and a "1" score to window chambers in which blood flow was no longer evident. We used dose-response analysis to calculate a characteristic radiant exposure ($RE_{50}/7$) at which 50% of irradiated window chambers are expected to have vascular shutdown on Day 7. (A-C) Representative LSI data associated with 595-nm PDL irradiation, in which persistent vascular shutdown was not (top) and was (bottom) achieved, using radiant exposures of (A) 4, (B) 6, and (C) 10 J/cm^2, respectively. (D) Based on data from 19 experiments, we identified a $RE_{50}/7$ of 7.1 J/cm^2 for PDL irradiation.

3.3.2 Combined use of PDT followed immediately by PDL irradiation resulted in persistent vascular shutdown at a significantly lower characteristic PDT radiant exposure.

We then conducted a set of experiments in which we varied PDT radiant exposure (20 to 60 J/cm^2) and then applied a PDL pulse at a radiant exposure (4 to 6 J/cm^2) below the PDL $RE_{50}/7$ value (Figure 3.1D). We used LSI to monitor the microvascular response to the PDT+PDL approach. We determined that the characteristic PDT radiant exposure required to achieve persistent vascular shutdown, decreased from 85 to 45 J/cm^2 (Figure 3.2). This difference in PDT $RE_{50}/7$ was found to be statistically significant ($p = 0.0002$).

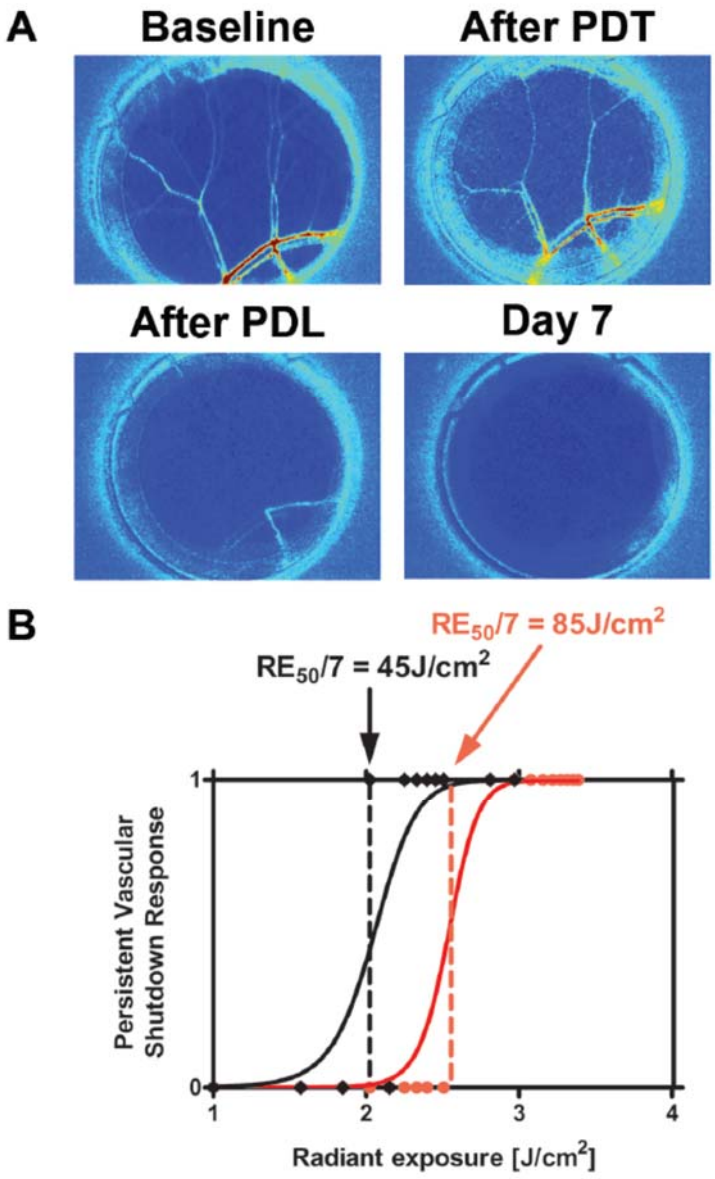

Figure 3.2 The combination of TS-mediated PDT and PDL irradiation leads to a significant reduction in the characteristic PDT radiant exposure required to achieve persistent vascular shutdown. In this set of experiments, we used PDT (20 to 60 J/cm^2) and PDL radiant exposures (4 to 6 J/cm^2) that were below the $RE_{50}/7$ values of 85 J/cm^2 (Moy et al., REF) and 7.1 J/cm^2 (Figure 1D), respectfully. (A) Representative maps of blood flow that demonstrate persistent vascular shutdown at Day 7. In this specific example, we applied PDT with a radiant exposure of 60 J/cm^2 followed by PDL irradiation at a radiant exposure of 6 J/cm^2. This combination resulted in marked acute vascular shutdown which persisted through Day 7. (B) Based on data from 30 experiments, we determined that the characteristic radiant exposure required to achieve persistent vascular shutdown, decreased from 85 J/cm^2 with PDT alone to 45 J/cm^2 for the combined PDT+PDL protocol.

3.3.3 The characteristic intravascular dwell time for Talaporfin sodium is ~22 min in the normal dorsal window chamber microcirculation.

To determine the location of photodamage induced by PDT, we next used intravital microscopy to study the pharmacokinetics of TS in our in-vivo preclinical model. We applied a two-compartment model to the measurements of TS fluorescence emission from specific regions of interest. Based on the model fit, we estimated a characteristic TS intravascular time of ~22 min in Figure 3.3, which suggests that persistent vascular shutdown is associated primarily with intravascular photodamage.

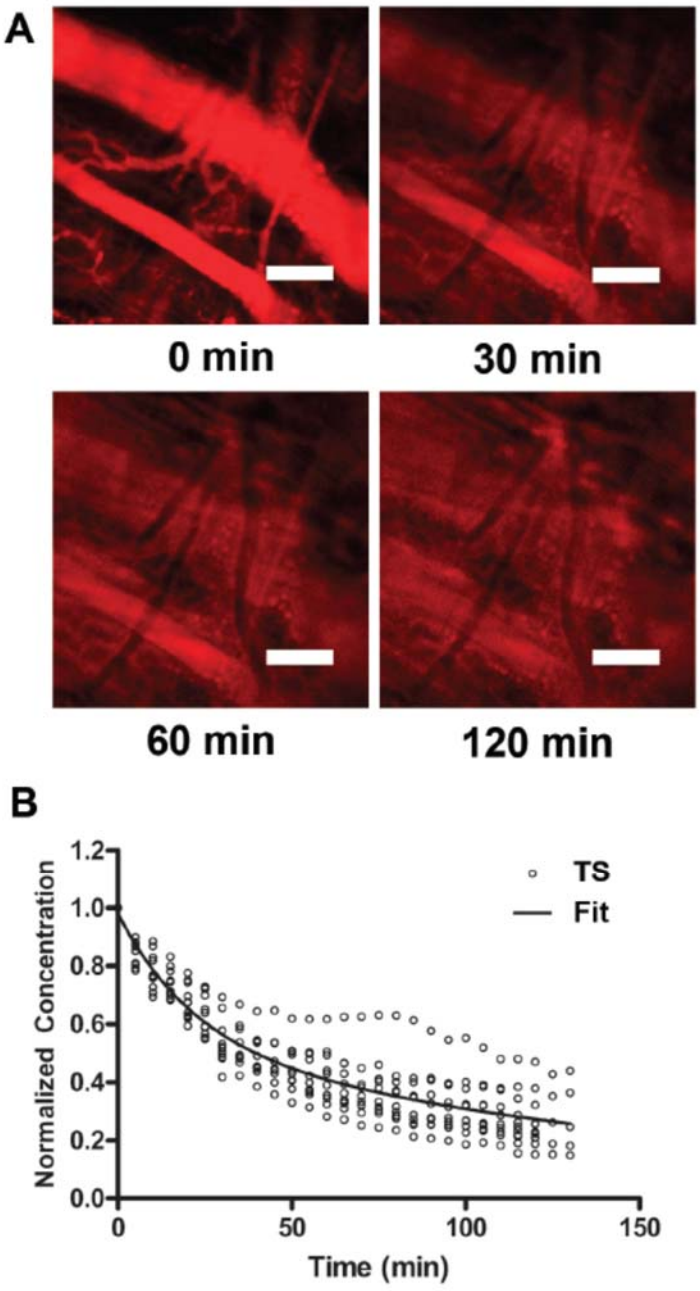

Figure 3.3 Application of two-compartment model to characterize the intravascular lifetime associated with TS. (A) We collected intravital microscopy images of fluorescence emission of TS from regions of interest in the window chamber. We observed a marked decrease in fluorescence within the initial 30 min and slower diffusion of TS out of the microcirculation into the perivascular space. Scale bar represents 300 μm. (B) Fluorescence emission data from specific regions of interest in window chamber preparations (n=11), and a best-fit curve associated with a double exponential, two-compartment pharmacokinetic model. Based on these data, we estimated that TS has a characteristic intravascular lifetime of ~22 min.

3.4 Discussion

Clinicians routinely use lasers to treat PWS. With PDL therapy, most patients require more than 15 sessions to achieve complete lesion removal[75]. Our group and others have studied the use of PDT as either an alternate or adjuvant method to treat PWS birthmarks[39-41, 43, 85]. Although recent preclinical and clinical results are promising, the optimal photosensitizer for vascular-specific PDT and the associated mechanism of action remains unknown. Our results 1) establish a characteristic radiant exposure ($RE_{50}/7$) to achieve persistent vascular shutdown with PDL irradiation (Figure 3.1); 2) reveal that combination PDT+PDL approach reduces the PDT light dose required to achieve persistent vascular shutdown, even at low PDL radiant exposures (Figure 3.2); and 3) suggest that TS-mediated PDT achieves persistent vascular shutdown primarily via endothelial cell damage (Figure 3.3).

We first set out to determine the PDL radiant exposures required to achieve persistent vascular shutdown. Similar to methodology used in previous studies of photocoagulation of microvasculature[69, 70, 85], we used dose-response methodology to estimate the $RE_{50}/7$ value required to induce persistent vascular shutdown following 595-nm PDL irradiation (10 mm spot; 1.5 ms pulse duration). Based on our experimental data, we estimated a $RE_{50}/7$ value of 7.1 J/cm^2 for PDL irradiation (Figure 3.1). Previously, we determined that the $RE_{50}/7$ value associated with TS-mediated PDT, using a custom-built LED array centered at 664 nm (FWHM = 20 nm), was 85 J/cm^2[85].

With the PDL and PDT $RE_{50}/7$ values established, we next studied the PDT radiant exposure required to achieve persistent vascular shutdown with the combined PDT+PDL approach. We focused our study on using PDL and PDT radiant exposures that both were

below the respective $RE_{50}/7$ values, based on the hypothesis that the combined PDT+PDL treatment will achieve effective blanching of the PWS with otherwise sub-therapeutic radiant exposures of PDT and PDL irradiation. Our data (Figure 3.2) demonstrate that the PDT $RE_{50}/7$ value required to induce persistent vascular shutdown with the combination PDT+PDL treatment protocol is substantially lower than the value required with PDT alone (45 vs. 85 J/cm^2, respectively).

Based on this result, we can evaluate the degree of synergy between the PDT and PDL vascular effects when the two phototherapies are combined. To assess the degree of interaction (α) between PDT and PDL irradiation, we employ a method described previously by Madsen et al[88]:

$$\alpha = \frac{f_{PDT}\, f_{PDL}}{f_{PDT+PDL}}$$

Where f_{PDT} and f_{PDL} are the fractions of PDT and PDL experiments, respectively, which do not induce persistent vascular shutdown, and $f_{PDT+PDL}$ is the fraction of combined experiments which do not induce persistent vascular shutdown. In this analysis, $\alpha = 1$ indicates an additive effect (or absence of any effect), $\alpha > 1$ indicates a synergistic effect, and $\alpha < 1$ indicates an antagonistic effect. We focused our analysis on the parameter space evaluated with the PDT+PDL experimental study (Figure 3.2): PDT radiant exposures of 20 to 60 J/cm^2[85] and PDL radiant exposures of 4 to 6 J/cm^2. Based on these data, we calculate $\alpha = 2.7$, indicating that PDT and PDL together achieve a synergistic treatment effect. Although the mechanisms for this synergistic shutdown effect remain unknown, we postulate that the reduction is associated with partial endothelial cell damage induced

during PDT, with subsequent PDL irradiation completing the photodamage process required to achieve persistent vascular shutdown.

As an initial study of the mechanism of action associated with TS-mediated PDT, we employed intravital fluorescence microscopy to study how the distribution of TS changes with time (Figure 3.3). Based on previous data on BPD pharmacokinetics published by Zhou et al[87], we applied a two-compartment model[86] to the fluorescence emission data. With the model fit, we estimated a characteristic intravascular time for TS of 22 min. The $RE_50/7$ values of 45 and 85 J/cm^2 are associated with irradiation times of 7.5 and 14.2 min, respectively. These data, combined with our analysis on degree of interaction, collectively suggest that TS-mediated PDT induces damage primarily to the endothelial cells, which in turn is expected to induce platelet aggregation and thrombosis.

Mitra and Foster[62] demonstrated that optical activation of TS accelerated extravasation of the photosensitizer from abnormal tumor vasculature. It is possible that our intravital microscopy data, collected in the absence of PDT, overestimated the characteristic intravascular time of TS in the microcirculation of the dorsal window chamber during PDT. Future experiments will study this issue.

Currently, an animal model with PWS-like vasculature does not exist. Nevertheless, previous studies utilizing the dorsal window chamber demonstrated correlation with studies on in vivo PWS skin. Barton et al[89] used the dorsal window chamber model to identify formation of methemoglobin with photothermal irradiation of blood. This observation was the basis for development of several clinical laser systems applicable for treatment of PWS that utilize innovative strategies to target methemoglobin. Babilas et al[15] performed intravital fluorescence microscopy of dorsal window chambers irradiated

with PDL. They demonstrated inability of the PDL to photocoagulate small blood vessels, which is in agreement with clinical observations[90]. Our group previously used this model to demonstrate the potential of BPD-mediated PDT+PDL treatment protocol for enhanced vascular shutdown[39, 40], which has also been demonstrated in our pilot clinical study[41]. Based on the results obtained previously[85] and within the current study, we have initiated an Investigational Review Board approved trial to evaluate TS mediated PDT+PDL for treatment of PWS. The clinical design involves varying drug and light dose for PDT over the course of the study. Our early clinical data have demonstrated a higher degree of vascular shutdown with TS-mediated PDT than we observed previously with BPD-mediated PDT[41].

The observed reduction in PDT and PDL radiant exposures required to induce persistent vascular shutdown when these two modalities are combined (PDT+PDL), indicate that the dual therapy might represent a potential new approach for effective treatment of PWS birthmarks. Future preclinical studies focusing on the microscopic effects at the level of the endothelial cells and associated hemodynamics within the microcirculation should provide more insight into the degree of synergy associated with the combined PDT+PDL treatment protocol.

Successful removal of PWS birthmarks in children is expected to eliminate the psychosocial damage inflicted by these lesions. Unfortunately, the current optical treatment protocols for PWS birthmarks are limited in their ability to achieve substantial blanching of PWS birthmarks with few treatments. Our preclinical PDT+PDL data presented herein suggest that complete vascular shutdown can be achieved with reduced

light doses, which is an important first step toward achieving a vertical leap in the clinical management of PWS birthmarks.

In conclusion, PDT+PDL induced persistent vascular shutdown at lower radiant exposures than either treatment alone and has the potential to provide safer and enhanced removal of cutaneous vascular lesions.

3.5 Acknowledgments

The work was supported in part by grants obtained from the National Institutes of Health (R01 HD065536), the National Institutes of Health Laser Microbeam and Medical Program (P41 EB015890), and the Arnold and Mabel Beckman Foundation. The authors thank Light Sciences Oncology for their generosity in providing us with TS. The authors thank Dr. Tom Foster (University of Rochester) for discussions involving TS-mediated PDT.

Chapter 4 - HEMOPORFIN-MEDIATED PHOTODYNAMIC THERAPY ON NORMAL VASCULATURE

We report our study of Hemoporfin-mediated photodynamic therapy, the most commonly used photosensitizer for PWS treatment in China. We utilized the rodent dorsal window chamber model and performed blood flow monitoring using laser speckle imaging (LSI). Speckle flow index (SFI) maps of day 7 time points were tabulated using dose response analysis. We draw direct comparisons between NPe6-mediated PDT and Hemoporfin-mediated PDT and demonstrate the efficacy of Hemoporfin-mediated PDT to cause persistent vascular shutdown within the blood vessels.

Abstract

Port-wine stain birthmarks are currently treated using a pulsed dye laser (PDL) combined with cooling of the skin. PDL treatment protocols utilize 585-595 nm wavelength light, where hemoglobin strongly absorbs this range of light. An alternative treatment option to the PDL is photodynamic therapy (PDT). The objective of the current study was to evaluate a PDT protocol that involves use of the most commonly used intravascular photosensitizer Hemoporfin for treatment of cutaneous vascular lesions, activated by a commercially available laser diode.

To monitor the microvasculature, a dorsal window chamber model was installed on 21 adult male mice. The light source consisted of a DSSP laser that emitted 150 mW at 532 nm. The light source was positioned at a set distance from the window chamber to achieve a fixed irradiance of 100 mW/cm^2. A retroorbital injection of Hemoporfin (2 mg/kg) was performed to deliver the drug into the bloodstream. Laser irradiation was initiated

immediately after injection. To monitor blood-flow dynamics in response to PDT, we used laser speckle imaging. We employed a dose–response experimental design to evaluate the efficacy of Hemoporfin-mediated PDT.

We observed four general hemodynamic responses to PDT: (1) At low radiant exposures, we did not observe any persistent vascular shutdown; (2) at intermediate radiant exposures, we observed delayed vascular shutdown effect with significant change to the vascular structure; (3) at intermediate radiant exposures, we observed an acute vascular shutdown effect with gradual restoration of blood flow and no significant changes to the vascular structure; and (4) at high radiant exposures, we observed acute vascular shutdown that persisted during the entire 7-day monitoring period, with no change in vascular structure. Dose–response analysis enabled identification of 359 J/cm^2 as a characteristic radiant exposure required to achieve persistent vascular shutdown at Day 7 following PDT.

The experimental data suggest that Hemoporfin-mediated PDT can achieve persistent vascular shutdown of normal microvasculature, but fairly high radiant exposures, or long treatments times, are required to achieve this effect.

4.1 Introduction

Port wine stain (PWS) birthmarks are congenital vascular malformations. Over 95% of PWS birthmarks are found on the face and neck regions[4]. Current treatment protocols in the US involve the use of a pulsed dye laser (PDL) combined with cooling of the skin[9]. Yellow light, in the 585–595 nm wavelength range, is strongly absorbed by hemoglobin and can photocoagulate the targeted vasculature.

An alternative treatment option to PDL therapies for PWS is photodynamic therapy (PDT). PDT contains three main components: 1) an optical light source, 2) photosensitizer, and 3) creation of cytotoxic singlet oxygen[91]. Excitation of the photosensitizer within the PWS blood vessels allows for specific targeted injury of vasculature. Today, PDT treatment for PWS is most commonly practiced by physicians in China, utilizing Photocarcinorin (PSD-007)[42] or Hemoporfin (HMME)[92, 93].

In 2007, Gu et al[42] published data collected from 1949 lesions in 1385 PWS patients treated with PDT. They found 128 cases (6.6%), after only 2 or more PDT session, resulted in full 100% clearance, and another 145 lesions (7.4%) had poor results with clearance <50%. Subjects treated with PDT were required to remain out of sunlight for 4 weeks. In 2011, Xiao et al[93] published data from 642 patients over a 5 year period, averaging 3-8 treatment sessions per person. They observed 5% of patients with complete clearing (100%), 29.8% of patients with more than 50% clearing, and over 70% of patients with more than 25% clearing. Ten percent of patients were reported to have experienced complications including blistering, hypopigmentation, hyperpigmentation, scarring, and photoallergy, for a time period <2 months. Patients were required to avoid sunlight 2 weeks after PDT, due to the long duration of photosensitivity. Results from multiple published studies on PDT treatment of PWS have indicated that PDT can be effective; however, a prolonged photosensitivity period and a large risk of scarring are side effects that must be taken into consideration.

In previously published studies, we investigated Benzoporphyrin Derivative Monoacid Ring A (BPD) and Talaporfin sodium (TS) as photosensitizers for vascular-specific PDT[39-41, 85] and for a combined PDT+PDL treatment protocol[94]. The

rationale to investigate a combined protocol was to utilize both treatments for a synergistic effect in treating PWS, while simultaneously minimizing the risks of each treatment by using lower energies. We investigated BPD because it has vascular specific properties and it is an FDA-approved clinical treatment for wet aged macular degeneration[76]. In a preclinical study involving an animal model, we conducted experiments to compare BPD-mediated PDT, PDL, and combined PDT+PDL treatment protocols over a five-day monitoring period to determine the efficacy of each treatment. We observed that the combined PDT+PDL protocol was the only consistent treatment that resulted in persistent vascular shutdown sustained over the entire duration of the monitoring period. We then translated these findings into a preliminary clinical study that evaluated the PDT+PDL protocol versus either PDT or PDL alone protocols[41]. No adverse events and mild epidermal changes in this study. We also observed visual improvement in the treated skin utilizing the combined protocol, but not the desired degree of blanching. We then moved to TS, which has been previously investigated for treatment in a number of indications: esophageal cancer, malignant gliomas, and lung cancer[78, 79, 82]. TS is a promising photosensitizer for PDT treatment for PWS due to its long intravascular dwell times[62] and has also been evaluated in multiple clinical trials that demonstrate evidence of safety and minimal adverse side effects in humans[78, 81-83]. TS has a reported photosensitivity period of one week, comparable to BPD[83], and has an absorption peak at 664 nm, which will enable treatment of both deep and superficial vasculature. Based off a 2009 study performed by Ohiro et al[84], involving the use of the rooster comb preclinical model of PWS vasculature, TS-mediated PDT was reported to induce blanching and be a possible treatment for cutaneous vascular lesions. In 2012, we evaluated TS-mediated PDT on the

dorsal window chamber model and determined a characteristic radiant exposure of 85 J/cm^2 is necessary for persistent vascular shutdown[85].

The objectives of the current study were to 1) establish a characteristic radiant exposure to achieve persistent vascular shutdown with Hemoporfin-mediated PDT, 2) determine if the Hemoporfin-mediated PDT light dose required to achieve persistent vascular shutdown is comparable to that of NPe6-mediated PDT, and 3) observe the mechanism of action associated with the Hemoporfin-mediated PDT protocol.

4.2 Materials and Methods

4.2.1 Dorsal window chamber model

Similar to previous work from our group[48, 85, 94], we utilized the dorsal window chamber model and performed experiments on adult C3H mice (25-30 g, n = 32). All experiments were approved by the Institutional Animal Care and Use Committee at University of California, Irvine.

4.2.2 Hemoporfin irradiation

For Hemoporfin-mediated PDT irradiation, we utilized a commercially available diode pumped solid state laser (532 nm Dragon Laser, Jilin, China). The light source was positioned to achieve an irradiance of 100mW/cm^2. The irradiation time was varied to achieve radiant exposures ranging 0-550 J/cm^2. Hemoporfin was reconstituted into a stock solution of 25 mg/mL. A retro-orbital injection of Hemoporfin (2 mg/kg) was performed to deliver the drug into the bloodstream and laser irradiation initiated immediately after injection. The drug dose was selected based on clinical treatment parameters found in review of clinically published results.

4.2.3 Experimental design

We anesthetized and positioned the animal in a custom window chamber holder placed on top of a heating pad. We irradiated the window chamber from the epidermal side. All experiments were randomized to minimize systematic bias.

4.2.4 Laser Speckle Imaging (LSI)

We monitored the photochemical effects of Hemoporfin-mediated PDT irradiation by observing blood flow dynamics using LSI. Briefly, a 633-nm Helium-Neon laser was used to illuminate the dermal side of the window chamber, from which raw speckle image sequences were collected. Using a simplified speckle imaging equation, we processed the collected images to Speckle Flow Index (SFI) images. LSI methodology has been previously described in detail[48].

4.2.5 Dose response analysis

Similar to previous publications[85, 94], we used the dose-response analysis approach. We performed 32 experiments for Hemoporfin-mediated PDT. We monitored blood flow in a longitudinal fashion to study the fate of the microvasculature following phototherapy. Raw speckle images were collected at the following time points: pre-phototherapy; immediately post-phototherapy; and at Days 1, 2, 3, and 7 after phototherapy. All authors (BC, WJM, GM, KK) independently reviewed the SFI images collected on Day 7 of each experiment and graded each set of images on a binary scale: a "0" (no persistent vascular shutdown on Day 7) or "1" (persistent vascular shutdown achieved on Day 7) was assigned to each Day 7 image. We used a commercial software package (Prism version 5.0d, GraphPad Software, San Diego, CA) to perform a sigmoidal fit

to the data and estimated a characteristic radiant exposure ($RE_{50}/7$) at which persistent vascular shutdown was achieved.

4.3 Results

We observed four general hemodynamic responses to Hemoporfin-mediated PDT (Figure 4.1, 4.2). At low radiant exposures, we observed no persistent vascular shutdown and no change in vascular structure. At intermediate radiant exposures, we either observed a delayed vascular shutdown effect, with significant change to the vascular structure, or we observed an acute vascular shutdown effect with gradual restoration of flow, and no significant changes to the vascular structure (Figure 4.2). At high radiant exposures, we observed acute vascular shutdown that persisted over the 7-day monitoring period, with no change vascular structure.

We utilized a previous grading system[85] and determined that 7 out of the 21 experiments produced a "0" result, while the remaining 14 experiments produced a "1" result at Day 7. There was not a clearly defined relationship between increasing radiant exposure and the expected result of persistent vascular shutdown.

Dose–response analysis enabled identification of 359 J/cm^2 as the $RE_{50}/7$ value for Hemoporfin, or the requisite energy needed to achieve persistent vascular shutdown at Day 7 following PDT (Fig. 4.3). At the 95% confidence interval, a range of 252–505 J/cm^2 was calculated for the $RE_{50}/7$ value.

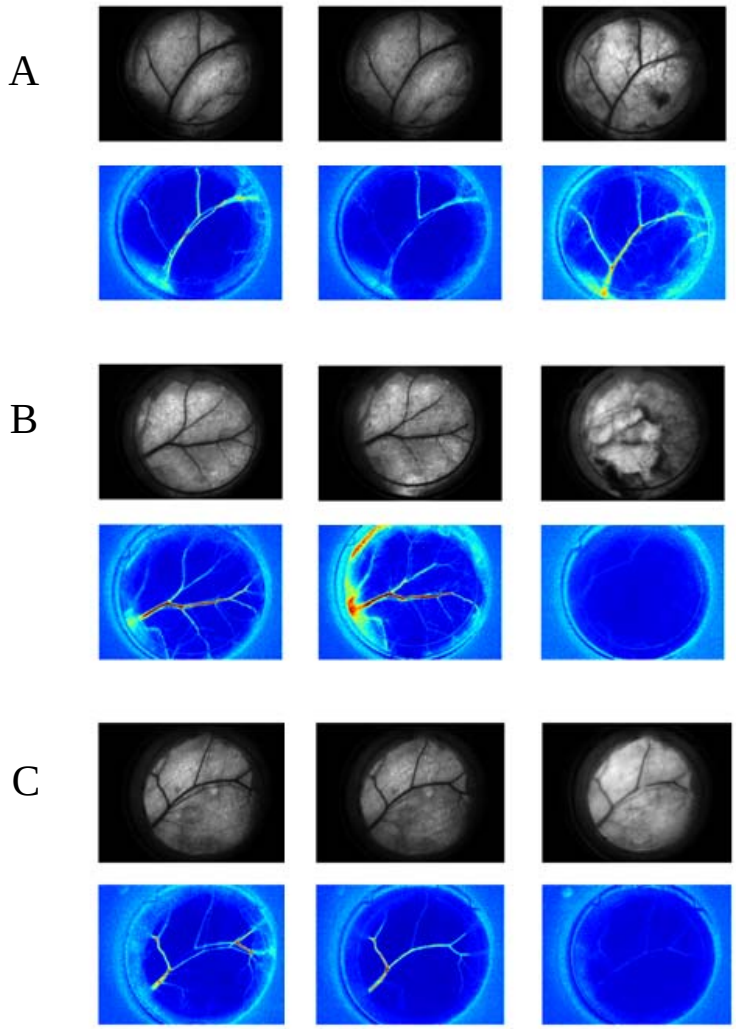

Figure 4.1 Observed trends within Hemoporfin-mediated PDT. Brightfield and SFI images are displayed at time points Day 0 pre-experimentation, Day 3 and Day 7. A) 33 J/cm^2 radiant exposure, showing no shutdown or reduction in flow with vasculature intact. B) 169 J/cm^2 radiant exposure, showing change in morphological structure of vasculature with complete shutdown. C) 300 J/cm^2 radiant exposure, showing no change in morphological structure of vasculature with complete shutdown. Presence of hemorrhaging was observed in all windows, as evidenced by fluctuations in background intensity and structural change in tissue surrounding vasculature.

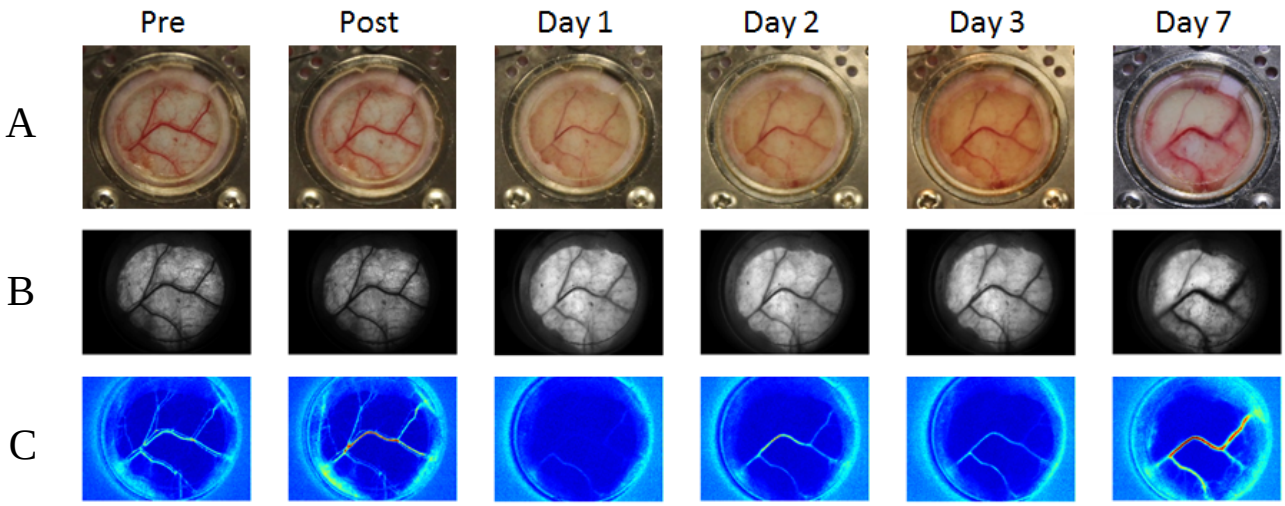

Figure 4.2 Representative example of Hemoporfin-mediated PDT using clinical conditions on preclinical model. We used 100 mW/cm^2 irradiance, 2 mg/kg drug concentration, and 133.8 J/cm^2 radiant exposure. We performed laser-mediated PDT on the epidermal side of window chambers and imaged blood-flow dynamics using LSI. We assessed persistent vascular shutdown on Day 7. We observed acute vascular shutdown, followed by gradual improved flow. We assigned a "0" score to for this experiment as there was evidence of blood flow recovery. A) Color and B) Brightfield images of the window chamber, indicating that blood vessel structure changed only minimally throughout 7 day monitoring. C) SFI images that display functional flow within the blood vessels of the window chamber. Flow was reduced through day 3 of the experiment, but returned at day 7

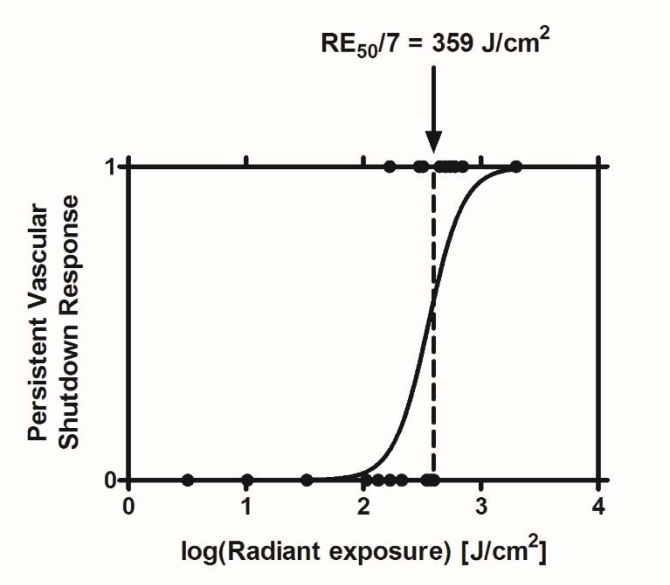

Figure 4.3 Hemoporfin-mediated PDT dose response curve. Based on data from 21 experiments, we identified a RE$_{50}$/7 of 366 J/cm^2.

4.4 Discussion

The experimental data (Figures 4.1, 4.2, 4.3) suggest that Hemoporfin-mediated PDT can achieve persistent vascular shutdown at doses greater than 359 J/cm^2, and we have verified that this approach can be used to cause persistent vascular shutdown, as it has been demonstrated in published clinical studies[46, 47, 92]. Further preclinical evaluation is warranted to better characterize the mechanism of injury, as it was observed to have a much delayed effect on the vasculature compared to the more immediate effect caused NPe6.

Analysis of high radiant exposures (>360 J/cm^2) revealed that Hemoporfin was consistent in the resultant persistent vascular shutdown. The vascular structures remained but did not have any functional flow. Hemoporfin-mediated PDT caused shutdown in both large and small blood vessels, leading to the quality of the window chamber degrading significantly by the end of the 7 day monitoring period. Thus, Hemoporfin-mediated PDT may be more effective in shutting down small diameter blood vessels that are not easily treated with the pulsed dye laser. However, PDT with this agent must be approached with caution as there will be significant potential for skin necrosis.

In our previous studies involving NPe6-mediated PDT, we determined a characteristic radiant exposure of 85 J/cm^2 and at 127mW/cm^2 irradiance, this equates to an irradiation time of 10 minutes. However, with the Hemoporfin-mediated PDT, at 100mW/cm^2, a 359 J/cm^2 treatment equates to 60 minutes, which may be difficult for patients to tolerate in the clinic. From previous published studies[46, 47, 92], we also examined clinically used parameters (100mW/cm^2 irradiance and 100 J/cm^2 radiant exposure) and evaluated them on the dorsal window chamber model. We found that

radiant exposures between 75-200 J/cm^2 yielded variable results, meaning some experiments produced persistent vascular shutdown, while others did not. Upon further examination of the dose response curve, the 95% confidence interval is large due to the fluctuating “0” and “1” scores over that energy range.

Similar to NPe6-mediated PDT, we observed the phenomena of acute vascular shutdown where blood flow was shut down immediately after treatment but gradually returned by Day 7 (Figure 4.2). However, one stark difference was the radiant exposure used that resulted in this effect (>369 J/cm^2 compared to 85J/cm^2 for NPe6), in addition to the lack of vascular structure change observed. One potential biological response mechanism is a restoration of the vascular network by reperfusion of blood vessels that were not entirely photocoagulated as a result of the Hemoporfin-mediated PDT. The observation of flow recurrence in some experiments confirms the need for monitoring beyond the 24 hour post-treatment mark. The immediate and acute vascular response can be subject to change and assessment of immediate changes in blood flow can lead to a misleading interpretation of the overall treatment outcome.

Our past work with NPe6[85, 94], demonstrates that translation of PDT experiments performed on rodents to humans must be carefully considered. Light doses required for the clinical response in humans[14, 43, 45-47, 92, 95] were found to be very different in the mouse model. We frequently observed tissue necrosis in the rodent model, which may be due to a lack of deep vasculature which did not occur in the clinical trial. The primary value we drew from the preliminary animal experiments was to confirm that persistent vascular shutdown can be achieved and that we can compare and contrast the amount of energy required to achieve the same type of results in each photosensitizer/light combination.

Previous studies of Hemoporfin-mediated PDT have demonstrated promising outcomes for PWS treatment[14, 43, 45-47, 92, 95]. Our current study of Hemoporfin-mediated PDT treatment highlights the effectiveness of this therapy for vascular shutdown but indicates that prolonged irradiation times are required and necrosis can occur.. Our future work will study the mechanism of injury caused by Hemoporfin-mediated PDT on vasculature and may include combination therapy with the PDL to see if there is a synergistic effect when the two treatment modalities are used together.

4.5 Acknowledgements

The work was supported in part by grants obtained from the National Institutes of Health (HD065536), the National Institutes of Health Laser Microbeam and Medical Program (LAMMP, project number P41EB015890), and the Arnold and Mabel Beckman Foundation. The authors thank Shanghai Fudan-Zhejiang Bio-Pharmaceuntical Co for providing the drug. The authors thank Dr. Austin Moy (The University of Texas at Austin) for assistance in preparing this manuscript.

Chapter 5 - STRUCTURAL CHANGES IN TISSUE DAMAGE ASSOCIATED WITH TALAPORFIN SODIUM-MEDIATED PHOTODYNAMIC THERAPY IN RAT SKIN

We report our study of Talaporfin sodium-mediated photodynamic therapy using a rat model and looking at histology and immunohistochemistry at 3 days post-treatment.. We investigated the mechanism by which Talaporfin Sodium-mediated PDT causes shutdown of blood vessels inducing apoptosis 9 hours post treatment. Depth of tissue and vascular injury are light dose dependent when drug concentration and irradiance are held constant.

Abstract

Alternative treatments are needed to achieve consistent and more complete port wine stain (PWS) removal, especially in darker skin types; photodynamic therapy (PDT) is a promising alternative treatment. We previously reported on Talaporfin Sodium (TS)-mediated PDT. It is essential to understand treatment tissue effects to design a protocol, which will achieve selective vascular injury without ulceration and scarring. The objective of this work is to assess skin changes associated with TS-mediated PDT with clinically relevant parameters.

We performed TS (0.75 mg/kg)-mediated PDT on Sprague-Dawley rats. Radiant exposures were varied between 15-100 J/cm^2. We took skin biopsies 3 days post-treatment. We assessed the degree and depth of vascular and surrounding tissue injury using histology and immunohistochemistry staining.

TS-mediated PDT at 0.75 mg/kg combined with 15 and 25 J/cm^2 light doses resulted in vascular injury with minimal epidermal damage. At light dose of 50 J/cm^2, epidermal damage was noted with vascular injury. At light doses >50 J/cm^2, both vascular and surrounding tissue injury were observed in the forms of vasculitis, extravasated red blood cells and coagulative necrosis. Wide spread coagulative necrosis involving deeper adnexal structures was observed in 75 and 100 J/cm^2 light doses. Observed depth of injury increased with increasing radiant exposure, although this relationship was not linear.

TS-mediated PDT can cause selective vascular injury; however, at higher light doses, significant extra-vascular injury was observed. This information can be used to contribute to design of safe protocols to be used for treatment of cutaneous vascular lesions.

5.1 Introduction

In the United States, port wine stain birthmarks (PWS) typically are treated with high intensity pulsed light. The pulsed dye laser (PDL, λ = 585-595 nm) combined with epidermal cooling of the skin is the most commonly used light source. Intravascular oxy- and deoxy-hemoglobin are selectively targeted by the PDL. The light energy is converted to heat, which causes localized vascular damage. Activation of the clotting cascade, and subsequent formation of thrombi, can lead to a severe reduction or complete shutdown of blood flow.

While PDL can lighten PWS, it is common to require 8-10 laser treatments or more[96]. Additionally, treatment of patients with darker skin is more difficult due to high epidermal melanin that competitively absorbs PDL light. In these patients, the maximum safe radiant exposure is lower due to the risk of damage to the epidermis, limiting treatment efficacy.

A clinical need exists to develop alternate or adjuvant treatment protocols. Photodynamic therapy (PDT), is a promising treatment option for PWS that involves the collective use of a photosensitizing agent, oxygen, and a light source to create the formation of cytotoxic singlet oxygen[42, 92, 93]. This approach has been used most commonly in China using Photocarcinorin and Hemoporfin as photosensitizers. However, the photosensitive period is 2 weeks or more and ulceration and scarring are significant risks.

We have endeavored to design alternative PDT protocols with a shorter photosensitive period and fewer side effects. Talaporfin Sodium (TS) in combination with 664 nm light is a promising option. We characterized blood flow changes associated with TS-mediated PDT on C3H strain mice[85] over a period of 7 days. 5 mg/kg of TS solution was administered via retroorbital injection. We determined a characteristic radiant exposure of 85 J/cm^2 for TS-mediated PDT. At radiant exposures >85 J/cm^2, we observed complete shutdown of perfusion, while below this range (<85 J/cm^2) blood flow either persisted or was temporarily shutdown before returning.

Type, extent and depth of TS-mediated PDT tissue injury has not previously been evaluated. In order, for TS-mediated PDT to be viable therapeutic option, injury should be limited to vasculature within 1-2 mm from the skin surface.

We hypothesize that TS-mediated PDT can cause selective vascular damage and the depth of this damage will be dependent on light dose. We administered 0.75 mg/kg of Talaporfin Sodium to Sprague Dawley rats, and varied the light dose (15-100 J/cm^2) and assessed the degree and depth of vascular and surrounding tissue injury using Hematoxylin and Eosin staining and immunohistochemistry staining. The 0.75mg/kg drug dosage differs

from previous studies (Moy, Kelly) utilizing a different preclinical animal model, as this new treatment parameters are currently being assessed in the clinical trial.

5.2 Materials and Methods

5.2.1 Sprague Dawley rat model

We performed experiments on male Sprague Dawley rats (200-250 g, n=10). We report on data collected from eight subjects, as two died before completion of the experiments. All experiments were approved by the Institutional Animal Care and Use Committee at University of California, Irvine.

5.2.2 Light source

We used a commercially available diode laser (664 nm, Biolitec AG). A 1000 um fiber (ocean optics, P1000-2-UV-VIS) delivered light from the laser to a beam expander (Thorlabs, BE10M-B), which produced a uniform 2 inch diameter collimated beam. Irradiance was measured using a handheld power meter (Coherent, PM3 device head, Molectron 3Sigma power meter), prior to irradiation.

5.2.3 Photosensitizer

We combined reconstituted TS (Light Sciences Oncology; Bellevue, Washington) with sterile saline to generate a stock solution of 25 mg/mL. We injected each subject with a dose of 0.75 mg/kg.

5.2.4 Fiber-based fluorescence probe

We monitored real time fluorescence from the TS solution injected into each animal. A laser diode (660 nm, 50 mW, Roithner laser, ADL-66505TL) was coupled to the center fiber of a 7-fiber fluorescence/reflection probe (Ocean Optics, R400-7-UV/VIS). The

surrounding 6 fibers were used for collection of the emitted fluorescence. Fluorescence emission was filtered using a razor edge filter (664 nm, Semrock, LP02-664RU-18-D) placed in an inline fiber optic filter holder (World Precision Instruments, 56200). Filtered emission was coupled through a fiber (Ocean Optics, 727-733-2447) directly into a spectrometer (Ocean optics, USB 2000) and analyzed using OceanView software (Ocean Optics, v1.4.0). The spectrometer exposure time was 40 ms, at a data collection rate of 0.5 Hz. Fluorescence data was analyzed by integrating over the collected spectrum from 650-850 nm.

5.2.5 Color photography and Microscopy

A commercial point and shoot camera (Canon EOS 5D Mark II, Canon EF 24-105mm F4 zoom lens) was used to take images of wound site progression on the rat model. Color photographs were taken of the animal prior to experimentation and application of the mask, after completion of PDT, and over the three-day monitoring period. Histological observations were made on a microscope (Zeiss Axioplan 2, Zeiss Plan-Neofluar objectives 20x/0.5 and 10x/0.3) and images were taken using a camera (Canon Power Shot G12).

5.2.6 PDT protocol

We used 5% isoflurane to induce anesthesia. The animal was placed onto a heating pad for body temperature regulation and was maintained under anesthesia with 3% isoflurane. We shaved and applied a depilatory cream (Nair, Church & Dwight, Marietta, GA) to the back side of each animal to reveal the skin. We identified three regions of interest on the back of each subject. We created a customized opaque mask containing three 1-cm diameter circles, with each circle spaced 5-mm apart in a triangular fashion (Figure 5.1). We used this mask to restrict PDT only to the regions of interest. We injected

a 0.75 mg/mL TS solution via tail vein injection into each subject. We placed the fluorescence probe onto the subject approximately 2 inches away from the treatment site. Once perfusion of the drug was identified by detecting TS fluorescence emission, PDT irradiation was initiated using the 664 nm laser. For all experiments, we used an irradiance of 100 mW/cm^2 and varied the irradiation time to achieve specific values of radiant exposure, 15, 25, 50, 75 and 100 J/cm^2. Three treatment spots with varying radiant exposures per subject were achieved by blocking specific regions of interest at predetermined time points during laser irradiation.

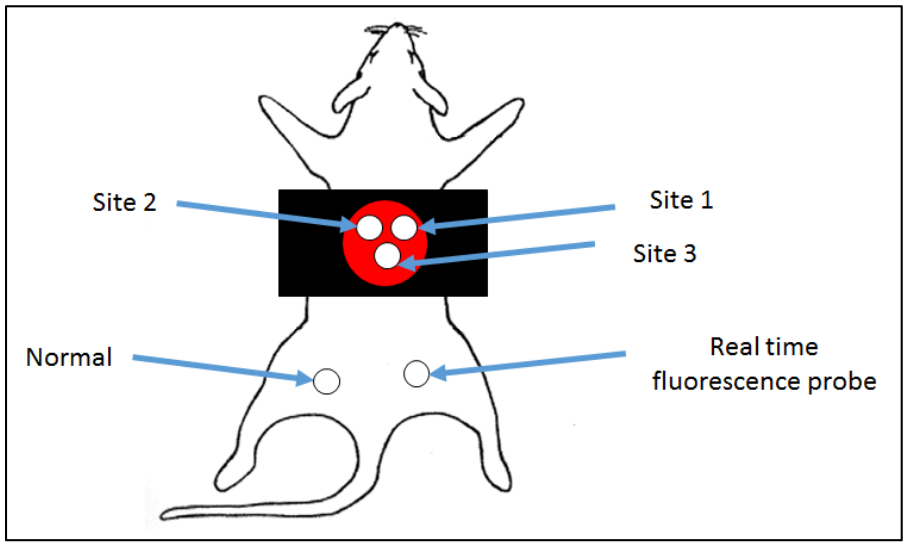

Figure 5.1 Schematic diagram of mask applied to dorsal side of rat. Sites represent where treatment occurred and where biopsies were taken. A fourth normal site, not exposed to any treatment light, was also biopsied. The real time fluorescence probe was placed approximately 2 inches from the mask, away from the treatment light.

5.2.7 Histology

Following color photography on day 0 (3, 6, 9, and 12 hour time points) and at day 3, we euthanized the subjects and collected 12 mm skin biopsies at each of the three treatment sites. A fourth site where no light treatment occurred was collected as a negative control. Biopsies included a border of normal, untreated skin surrounding the affected

treated area. Tissues were placed in 5% formalin and processed for histological analysis. Prior to embedding, the tissues were sliced through the middle of the sample and then embedded into paraffin wax. After embedding, three 10 μm thick tissue sections were removed from the tissue block and were stained with hematoxylin and eosin (H&E). Two board certified dermatopathologists (JY, SD) reviewed the H&E stained slides of TS-mediated PDT treatment spots from each animal. For 3, 6, 9, and 12 hour time points on day 0, immunohistochemistry stains Caspase 3 and CD31 were performed (Figure 5.4)

In order to quantify a positive Caspase 3 stain, the dermatopathologists rated each slide using a grade of 0-3 scale for color and quality of each stain: Grade 0: no staining, Grade 1: faint staining comparable to background non-specific staining of surrounding tissue; Grade 2: red, moderately intense staining; and Grade 3: bright red intense staining. To be considered a positive stain, the Capsase 3 antibody must show strong diffuse to punctate cytoplasmic staining of a Grade 2 and 3. Non-specific, thus negative staining, is noted with weak Grade 1 staining intensity or non-ceullar staining pattern such as staining of lumen of the vessels or stromal staining at the edge of the tissue sample.

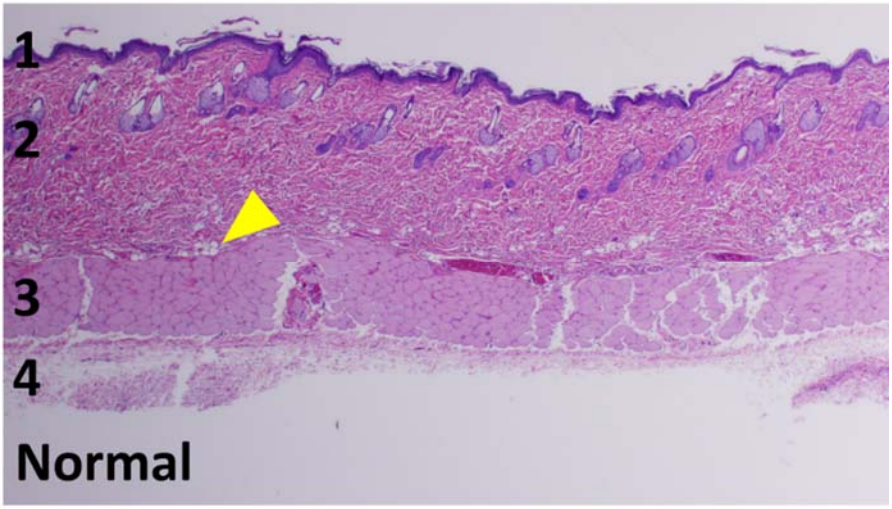

Figure 5.2 Hematoxylin and Eosin stained slide of normal skin. 1) Healthy epidermis that is 4-6 cells thick. 2) Dermis contains adnexal structures surrounded by delicate medium sized collagen fibers, deep in dermis lies a thin layer of stratum liposum, composed of aggregate of uniform adipocytes. 3) Stratum carnosus composed of bundles of skeletal muscle. 4) Stratum fibrosum consists of thicker caliber vessels mixed with stroma and wispy collagen fibers. Yellow arrow indicates artifact from H&E staining process.

5.3 Results

Normal Control: The epidermis, dermis, and subcutaneous layers in the normal control had structural features characteristic of normal tissue (Figure 5.2). The epidermis had a 4-6 cell thick layer of stratified squamous epithelium. The dermis was comprised of thin wispy collagen at the superficial layer and uniformly distributed adnexal structures (i.e. hair follicles, sweat glands), surrounded by medium sized collagen consistent with normal dermis. In the deep dermis lies a thin layer of stratum liposum, composed of aggregate of uniform adipocytes. The stratum fibrosum consists of thicker caliber vessels embedded in a loose stroma composed of wispy collagen fibers. Caspase 3 expression in normal skin was demonstrated by non-specific staining throughout the upper dermis (Figure 5.4A)

15 J/cm^2: At 15 J/cm^2 radiant exposure, the tissue exhibited minimal and limited structural changes from the normal control. Subcorneal micro-pustules, mild dermal edema, and focal epidermal erosion were noted in all samples. The average depth of tissue necrosis was noted to be 0.12 mm from the top of the epidermis.

25 J/cm^2: At 25 J/cm^2 radiant exposure, the epidermis showed minor erosion and was more pronounced and widespread than at 15 J/cm^2. Blood vessels in the dermis were observed to have early signs of ectasia and endothelial swelling. The average depth of tissue necrosis was 0.56 mm from the top of the epidermis (Figure 5.3B). On Day 0 at 9 hours, Caspase 3 expression revealed specific staining of superficial vessels in the upper dermis (Figure 5.4B). Non-specific staining was observed in vessels above the adipocytes (Figure 5.4C).

50 J/cm^2: At 50 J/cm^2, ulceration of the epidermis into the mid dermis was observed. Ischemic necrosis of the entire follicular structure was noted. Adjacent, blood vessels began to show signs of structural distress and some intravascular thrombi were noted. Early vasculitis was noted with neutrophils in the wall of the small caliber vessels; however, minimal extravasated blood cells were observed, indicating that the blood vessels were mostly intact. There was a mild chronic inflammatory response and some neovascularization in the stratum fibrosum. The average depth of tissue necrosis was 1.64 mm (Figure 5.3C).

75 J/cm^2: At 75 J/cm^2, the epidermis was completely eroded and the dermis was further damaged. The ischemic change involved the entire dermis to the level of the skeletal muscle. Dermal blood vessels were severely damaged. Pronounced vasculitis was noted with extravasated red blood cells. Significant neovascularization and a brisk

fibroblastic proliferation were noted, representative of a mild and early wound healing response. The average depth of tissue necrosis was 2.04 mm (Figure 5.3D). On Day 0 at 9 hours, Caspase 3 expression was observed in vessels at the superficial dermis and near the stratum fibrosum, in addition to a higher density of Caspase 3 expression overall (Figure 5.4D).

100 J/cm^2: At 100 J/cm^2, the epidermis was completely eroded and dermal necrosis extended into the skeletal muscles. In the dermis, the blood vessels were completely obliterated and extravasated red blood cells were pronounced. Prominent neovascularization and a significant fibroblast population were observed as well, indicating a brisk wound healing process. The average depth of tissue necrosis was 2.22 mm.

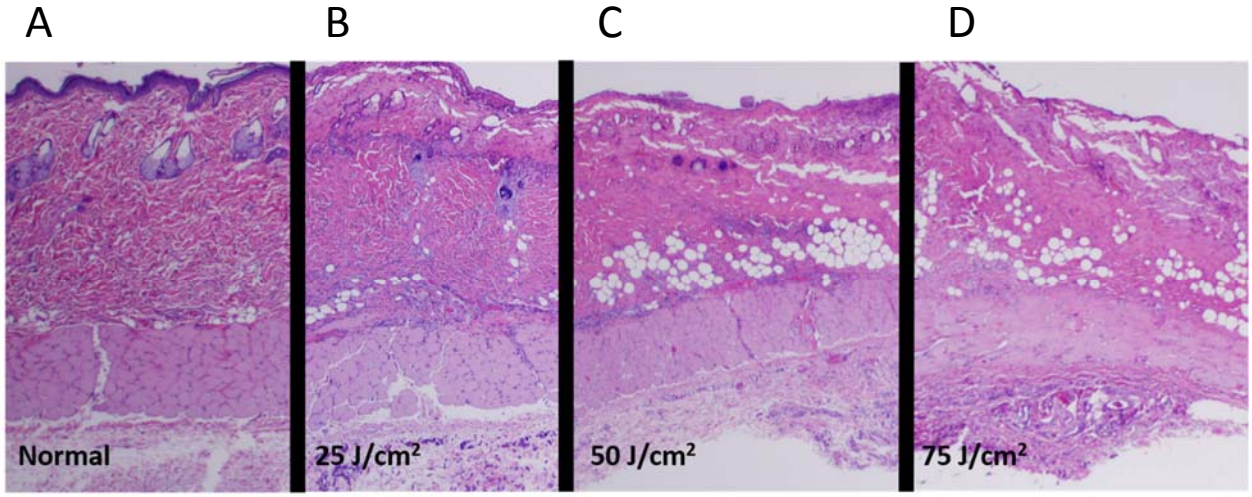

Figure 5.3 Hematoxylin and Eosin stained slides of normal, and TS-mediated PDT treated rat skin at 25, 50 and 75 J/cm^2 light doses. A) Normal rat skin, biopsy taken from site not exposed to light during PDT treatment. B) At 25 J/cm^2, a distinct line of neutrophils indicates the depth of necrosis, measured at 0.56mm. Vascular changes were observed in the superficial dermis, with minimal epidermal erosion. C) At 50 J/cm^2, the depth of tissue necrosis was measured at 0.56mm, a direct result from ischemic necrosis caused by vascular damage. Changes in vasculature were noted below the superficial dermis, in the form of extravasated red blood cells and thrombus formation. D) At 75 J/cm^2, ulceration and necrosis was noted from the epidermis through the mid stratum carnosus. Affected striated muscle was observed to have no nuclei, adjacent to healthy striated muscle with nuclei present. Vessels observed were severely damaged, with fibroblast and macrophage proliferation were noted in damaged tissue areas.

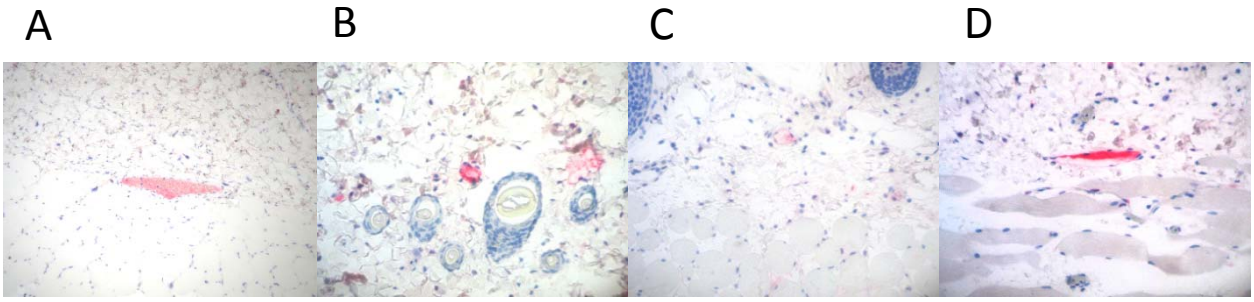

Figure 5.4 Caspase 3 stained slides of normal, 25 and 75 J/cm^2 on Day 0, 9 hour time point. A) Normal skin showing non-specific staining of blood vessel at 140x magnification. B) At 25 J/cm^2, specific staining of vessel showing endothelial cell damage at 70x magnification. A properly stained blood vessel is observed in the middle of the image, where the endothelial cells are undergoing apoptosis. C) At 25 J/cm^2, Non-specific staining of blood vessel above layer of adipocytes at 140x magnification. Stain is faint in color, and the stain highlighted non-cellular structures, the lumen of the vessel. D) At 75 J/cm^2, Caspase 3 specific staining of deep vessels noted above the adipocyte layer. Stain was scored at 3 (dark red color), endothelial cells were undergoing apoptosis and shape of vessel was uncompromised.

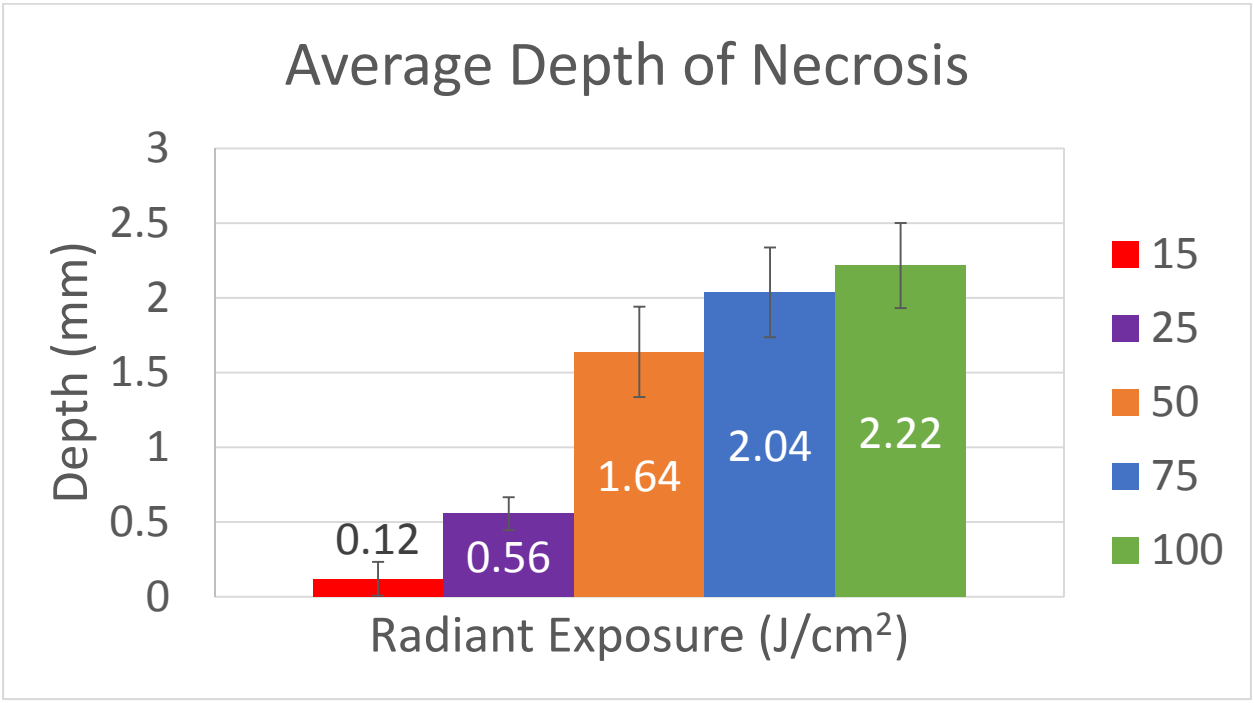

Figure 5.5 Average depth of necrosis observed at each radiant exposure. At least 5 depth measurements were made from each biopsy at the corresponding radiant exposure. Error bars indicate the standard deviation over the measurements made.

5.4 Discussion

Our results indicate that the severity and depth of injury is light dose dependent (Figures 5.3 and 5.4). This is expected and is nicely demonstrated by our results. There is a direct relationship between the dose and the amount and grade of epidermal injury, vascular damage and extra-vascular dermal changes. At 15 J/cm^2, there appears to be minimal tissue damage to the epidermis but no significant vascular injury and no injury to the surrounding dermis. At 25 J/cm^2, there appears to be minimal tissue damage to the epidermis, while vascular injury was noted in the Caspase 3 stain in the upper portion of the dermis. No injury was observed in the surrounding dermis. There is a pronounced increase in tissue damage severity and depth of injury starting at 50 J/cm^2, which is further observed with increasing light dosage. Dermal fibrosis and granulation tissue were noted at the level of the stratum carnosus for all doses 50 J/cm^2 and above.

At the dose of 50 J/cm^2, epidermal erosion was observed followed by vascular damage in the form of endothelial swelling. Mild fibroblastic proliferation was observed, indicating dermal wound response. At 75 J/cm^2, epidermal erosion was pronounced over the treatment site. Vascular damage was noted in the form of endothelial swelling. There was proliferation of fibroblasts to the injury site. On Day 0 at 9 hours, Caspase 3 staining revealed selective deep vascular damage (deep dermis above adipocyte layer), with an increase in Caspase 3 staining of the stromal fibroblasts as a result of increased damage to the surrounding tissue. At 100 J/cm^2, the epidermis was completed eroded, followed by deep vascular damage through the stratum fibrosum. Significant surrounding tissue damage was noted in the form of ischemic necrosis.

At higher doses (75 and 100 J/cm^2) there was pronounced granulation tissue with prominent neovascularization highlighted by small caliber, single layer vessels with luminal red blood cells. Vascular destruction and necrobiosis and collagen degeneration also occurred. Neovascularization, the process by which new vessels are formed, was prominent in the dermis-stratum carnosus interface. At 75 J/cm^2, damage was observed at the mid stratum carnosus level. At 100 J/cm^2, damage occurred from the epidermis through the stratum fibrosum. A high level of fibroblast proliferation was noted compared to the normal sample. Neovascularization was also prominent in the stratum fibrosum.

Figure 5.5 summarizes the tissue depth of injury observed at each radiant exposure. While the average depth is not linearly dependent on the light dosage, we see a clear relationship between increasing depth and increasing radiant exposure. Thus it is paramount to determine safe levels of light dosage to avoid wide spread tissue damage as observed in the highest radiant exposure (100 J/cm^2).

The rat skin model has significantly different characteristics compared to regular human skin and diseased port wine stain skin. The main differences include a lack of keratinized outer layer of skin in rats, skin thickness is much thinner in rats, and the number and density of blood vessels found in the superficial dermis. Despite these differences, the rat model allowed us to characterize and understand the effects of TS-mediated PDT at clinically relevant doses. Further investigation is warranted to determine if changing parameters can be more effective in selectively targeting vasculature.

It has been demonstrated that TS-mediated PDT can cause selective vascular injury; however, at higher light doses, significant extra-vascular injury was observed in the rat

model. This information can be used to contribute to design of safe protocols for treatment of cutaneous vascular lesions.

In conclusion, we have demonstrated a clear correlation between the administered light dose and the depth and extent of tissue injury during TS-mediated PDT. Future studies would involve taking biopsies at different time points to identify possible mechanisms, use of additional immunohistochemistry stains, and comparison with other photosensitizers.

5.5 Acknowledgements

The work was supported in part by grants obtained from the National Institutes of Health (R01HD065536), the National Institutes of Health Laser Microbeam and Medical Program (P41EB015890), the Arnold and Mabel Beckman Foundation, and the ASLMS Student Research Grant. The authors would also like to acknowledge Dr. Austin Moy (The University of Texas at Austin) for guidance and preparation of this manuscript. The authors would also like to acknowledge Dr. Kim Green, Dr. Monica Elmore, Dr. Sean White and Ben Lertsakdadet for their assistance with this project.

Chapter 6 - TARGETED NARROWBAND INTENSE PULSED LIGHT ON CUTANEOUS VASCULATURE

We report our study of Intense Pulsed Light (IPL), an alternative light based treatment to the Pulsed Dye Laser (PDL). We utilized the rodent dorsal window chamber model and performed blood flow monitoring using laser speckle imaging (LSI). We draw direct comparisons between PDL and this IPL device and demonstrate the efficacy of the IPL to cause persistent vascular shutdown within normal vasculature. Monte Carlo modeling was performed over the output spectrum of the IPL device and was compared to the PDL (595nm wavelength) to investigate the distribution of absorbed energy in a simulated blood vessel.

Abstract

Laser based therapies are the standard treatment protocol for port wine stain in the United States, but complete removal is infrequently achieved. Intense pulsed light (IPL) offers a broadband light spectrum approach as a viable treatment alternative. Previous studies suggest that IPL can be more effective in treatment of port wine stain by utilizing multiple wavelengths to selectively target different peaks in oxy- and deoxy-hemoglobin. Our study objectives were to 1) determine a characteristic radiant exposure able to achieve persistent vascular shutdown with narrowband IPL irradiation, 2) determine the degree to which narrowband IPL irradiation can achieve persistent vascular shutdown, and 3) compare the effectiveness of narrowband IPL radiation to single wavelength pulsed dye laser (PDL) irradiation in achieving persistent vascular shutdown.

We utilized either single pulse or double, stacked pulses in narrowband IPL experiments, with the IPL operating over a 500-600 nm wavelength range on the rodent dorsal window chamber model. We compared the results from our narrowband IPL experiments to acquired PDL data from a previous study and determined that narrowband IPL treatments can also produce persistent vascular shutdown. We ran Monte Carlo simulations to investigate the relationship between absorbed energy, wavelength, and penetration depth.

For single and double pulse narrowband IPL irradiation we observed 1) little to no change in blood flow, resulting in no persistent vascular shutdown; 2) marked acute disruption in blood flow and vascular structure, followed by partial to full recovery of blood flow, also resulting in no persistent vascular shutdown; and 3) immediate changes in blood flow and vascular structure, resulting in prolonged and complete vascular shutdown. Monte Carlo modeling resulted in a 53.2% and 69.0% higher absorbed energy distribution in the top half and the total simulated vessel when comparing the composite narrowband IPL to the 595 nm (PDL), respectively.

Our data collectively demonstrate the potential to achieve removal of vascular lesions using a 500-600 nm range. Additionally, the narrowband IPL was tuned to optimize a specific wavelength range that can be used to treat PWS, whereas the PDL can only operate at one discrete wavelength.

6.1 Introduction

Port Wine Stains (PWS) are vascular malformations of the skin that are birthmarks. PWS are characterized by an increase in vessel diameter (vasodilation) and increase in the number of blood vessels (hypervascularization)[97]. PWS lesions initially present as a

reddish pink coloration of the skin and are flat in nature. If left untreated, PWS often develop nodules and tissue hypertrophy[98], and can lead to dental abnormalities and psychosocial problems[7].

The standard treatment in the United States of PWS utilizes high intensity light, typically delivered by a laser, to selectively target abnormal vasculature. Clinicians often use the pulsed dye laser (PDL, λ = 585-595 nm), in conjunction with epidermal cooling[99], to minimize the amount of surrounding tissue damage caused by the thermal energy of the laser. The PDL is selectively absorbed by oxy- and deoxy-hemoglobin in blood vessels[7, 8] and subsequently is converted to heat that ideally reaches temperatures that create localized damage. Subsequent thrombosis formation leads to either a severe reduction in or shutdown of blood flow[74]. This entire treatment protocol is known as selective photothermolysis[100].

While PDL therapy of PWS has led to successful lightening of the PWS color, patients may require several laser treatments[75] before seeing sufficient improvement. PDL treatments can span over the course of many years, depending on the severity of the PWS disease, and its resistance to the PDL treatment. Furthermore, PDL therapy is not as effective for PWS patients with darker skin due to the competitive absorption of the laser light by epidermal melanin. As a result, the maximum radiant exposure must be decreased in consideration of tissue damage and safety concerns, which in turn limits the effectiveness of laser treatment.

Here, we investigated the use of targeted narrowband intense pulsed light (IPL) as an alternative light source to the PDL to determine if a range of wavelengths is more effective than the single wavelength from the PDL. A previous study of PDL-resistant

PWS[101] suggested that IPL (555-950 nm wavelength range) could be used as an alternative to the PDL. In this study, all subjects (n =15), with PWS of various sizes, locations and colors, achieved at least a 50% reduction of their PWS through IPL treatments. Another study conducted in China investigated the treatment of 30 PWS patients with IPL[102], operating over 515-1200 nm wavelength range with 3-8 treatment sessions over a duration of 4-5 weeks. They reported that 100% of patients showed more than 25% clearance, while 30% of patients were able to achieve 75% clearance, further showing that IPL, under certain treatment parameters, has the potential to be an effective treatment for PWS clearance both in a reduction in the number of treatments and improved efficiency of the treatment. A split-face study performed using the PDL and IPL[103] demonstrated that an IPL with a wavelength range of 555-950 nm achieved more effective clearance than the PDL (λ = 585 nm). Additionally, data from other studies[104, 105] suggest that IPL is a viable option for PWS clearance, but acknowledge that, due to the large variance in treatment parameters (pulse duration, radiant exposure, wavelength range), IPL warrants further investigation.

In this study, we used a narrowband IPL that emits broadband light over the wavelength range of 500 to 600nm. The wavelength range of this narrowband IPL enables light absorption over the entire absorption spectra of oxy- and deoxy- hemoglobin, including the 577 and 600 nm oxyhemoglobin absorption peaks while not using much higher wavelengths (900-1200 nm), which may enhance PWS clearance[106]. The objectives of the current study were to 1) determine a characteristic radiant exposure able to achieve persistent vascular shutdown with narrowband IPL irradiation, 2) determine the degree to which narrowband IPL irradiation can achieve persistent vascular shutdown, and

3) compare the effectiveness of narrowband IPL radiation to single wavelength PDL irradiation in achieving persistent vascular shutdown.

6.2 Materials and Methods

6.2.1 Dorsal window chamber model

Similar to previous work from our group[85, 94], we utilized the dorsal window chamber model[48] and performed experiments on adult C3H mice (25-30 g, n = 41). All experiments were approved by the Institutional Animal Care and Use Committee at University of California, Irvine.

6.2.2 IPL irradiation

For narrowband IPL irradiation, we utilized a commercially availble IPL (Dye-VL, Alma Lasers US, Buffalo Grove, IL) with a spot size of 10 mm, pulse duration between 3 and 5 ms and radiant exposure between 7 and 15 J/cm^2. A 15 mm diameter, 1-2 mm thickness of ultrasound gel was placed on the epidermal side of the window chamber, prior to contact with IPL device.

6.2.3 Experimental design

We anesthetized and positioned the animal in a custom window chamber holder placed on top of a heating pad. We irradiated the window chamber from the epidermal side with either a single pulse or two stacked pulses of narrowband IPL. For the latter (i.e., double-pulse) narrowband IPL experiments, a one-second delay was used between administration of the first and second pulses. All experiments were randomized to minimize systematic bias.

6.2.4 Laser Speckle Imaging (LSI)

We monitored the photothermal effects of the IPL irradiation by observing blood flow dynamics using LSI. Briefly, a 633-nm Helium-Neon laser was used to a illuminate the dermal side of the window chamber, from which raw speckle image sequences were collected. Using a simplified speckle imaging equation[53], we processed the collected images to Speckle Flow Index (SFI) images. LSI methodology has been previously described in detail[48].

6.2.5 Experimental design

Similar to previous publications[85, 94], we used the dose-response analysis approach. We performed 40 experiments for IPL irradiation with either a single (n = 13), or double (n = 27) pulse of light. We monitor blood flow in a longitudinal fashion to study the fate of the microvasculature following phototherapy[66]. Raw speckle images were collected at the following time points: pre-phototherapy; immediately post-phototherapy; and at Days 1, 2, 3, and 7 after phototherapy. Five of the authors (BC, WJM, COO, JDY, and JS) independently reviewed the SFI images collected on Day 7 of each experiment and graded each set of images on a binary scale: a "0" (no persistent vascular shutdown on Day 7) or "1" (persistent vascular shutdown achieved on Day 7) was assigned to each Day 7 image. We used a commercial software package (Prism version 5.0d, GraphPad Software, San Diego, CA) to perform a sigmoidal fit to the data and estimated a characteristic radiant exposure ($RE_{50}/7$) at which persistent vascular shutdown was achieved.

6.2.6 Monte Carlo modeling

A Monte Carlo computational model incorporating the window chamber, multiple layers of tissue, and a flat circular source profile was developed to estimate the absorbed

energy deposition in a vessel embedded within the hypodermis (Fig. 1). We simulated light propagation from 500 to 600 nm, in steps of 5 nm. The source was 5 mm in radius and assumed incident normal to a four-layer system comprised of skin, hypodermis, water and glass, to mimic the layers found in the window chamber. Within the hypodermis layer, a vessel with radius 81 μm was embedded. This vessel radius was selected based on calculation of the mean vessel radius determined from LSI images of 60 window chambers. The optical properties for each region are given in Table 6.1. The absorption coefficients for the skin, hypodermis and vessel were determined using the volume fractions of blood, water, blood oxygen saturation, and fat for each wavelength[107-109]. The scattering coefficient was determined from previous studies[108]. The Monte Carlo simulations were performed using used the Virtual Tissue Simulator software (http://virtualphotonics.codeplex.com). Photons were launched from the source and propagated within a conventional Monte Carlo simulation using discrete absorption weighting[110, 111], which deposits absorbed energy at each collision. The tissue was subdivided into 10 μm × 20 mm × 10 μm voxels along the x−, y− and z−axes to collect the absorbed energy; in other words, the vessel was modeled as a cylinder of infinite length. For each simulation, 106 photons were used which ensured that the relative errors of the absorbed energy estimates within the vessel, due to statistical noise associated with Monte Carlo modeling, were less than 2%.

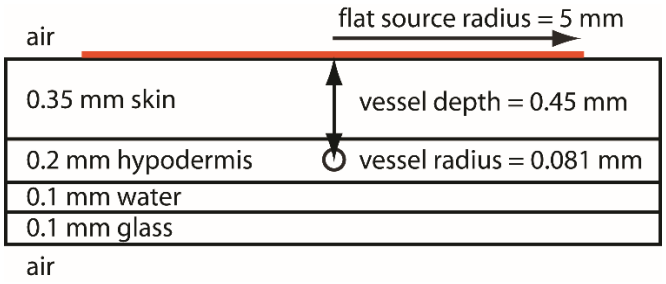

Figure 6.1 Schematic of geometry used to represent the dorsal window chamber in Monte Carlo simulations. Not drawn to scale. A depth position of 0mm represents the air-skin interface. The center of the 0.081mm radius vessel is at a depth of 0.45mm.

region	g	n	μ_s/mm	μ_a/mm
air	1	1.4	10^{-10}	0
skin	0.81	1.44	λ-varied	λ-varied
hypodermis	0.69	0.8	λ-varied	λ-varied
water	1.0	1.33	0.5704	0
glass	1.0	1.46	0.5704	0
vessel	0.98	0.8	λ-varied	λ-varied

Table 6.1 Tissue properties used in Monte Carlo simulations. Anisotropy (g), index of refraction (n), absorption (μa) and scattering (μσ) coefficients were based on values obtained from literature and are wavelength dependent.

6.3 Results

6.3.1 Single pulse narrowband IPL irradiation

Similar to trends observed previously with photodynamic therapy[85] and PDL irradiation[94] of the microvasculature in the window chamber, we observed three trends in the single pulse narrowband IPL irradiation data: 1) little to no change in blood flow over the 7 day monitoring period resulted in no persistent vascular shutdown; 2) marked acute disruption in blood flow and vascular structure, followed by partial to full recovery of blood flow over the 7 day period, which also resulted in no persistent vascular shutdown; and 3) immediate changes in blood flow and vascular structure, followed by prolonged and complete vascular shutdown by day 7. For experiments that did not result in persistent vascular shutdown, we observed the presence of hemorrhage within the window chamber

62% of the time (Table 6.2). Note that in Table 6.2, we present the data as irradiance (kW/cm^2) instead of radiant exposure, due to the different pulse durations used in this study. With an irradiance greater than 5333 kW/cm^2, we observed consistent, persistent vascular shutdown.

6.3.2 Double pulse narrowband IPL irradiation

With double-pulse narrowband IPL irradiation, we observed the same three trends as described above for the single pulse narrowband IPL irradiation data. We observed hemorrhage formation within the window chamber in 93% of experiments. Although hemorrhage formation did not correlate with persistent vascular shutdown, double pulse narrowband IPL irradiation induced persistent vascular shutdown at lower irradiance values (2000-4000 kW/cm^2) than single pulse irradiation (Table 6.2).

6.3.3 Monte Carlo Modeling

The results of the 20 simulations performed between 500-600 nm in 5 nm increments are displayed in Figure 6.2A. We calculated a composite absorbed energy distribution from the narrowband IPL simulations, with weighted contributions from each wavelength dependent on the narrowband IPL spectrum. Absorbed energy distribution is 53.2% higher in the top half of the composite narrowband IPL compared to the 595 nm (PDL). Total absorbed energy distribution over the entire simulated vessel is 69.0% higher in the composite narrowband IPL compared to the 595 nm (PDL). We performed further analysis in Figure 6.2C, in which a line profile of the normalized total energy absorption profile at 595 nm was compared to the combined total absorbed energy of the narrowband IPL. With 595 nm irradiation, we observed that the average absorbed energy is more

uniformly distributed over the diameter of the vessel than it is with narrowband IPL irradiation.

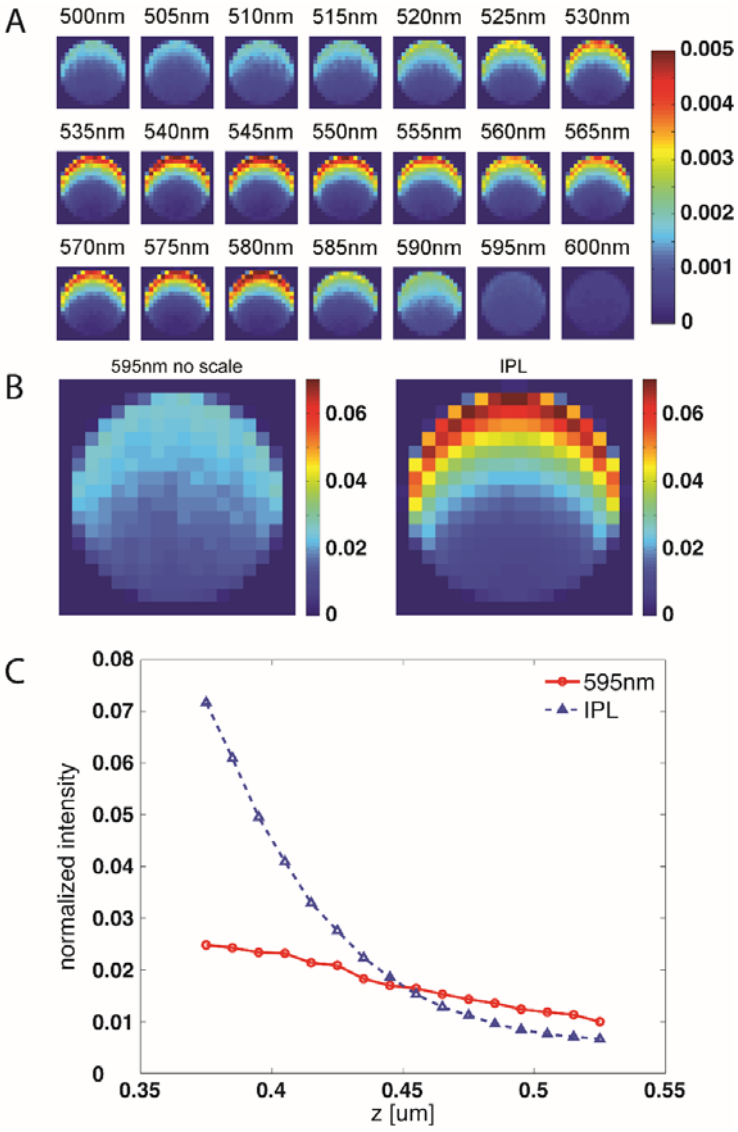

Figure 6.2 A) Normalized absorbed energy distribution within 0.081μm radius vessel over 500-600 nm wavelength range at 5 nm increments. All energy distribution maps are plotted on the same color scale. B) Comparison of 595 nm normalized absorbed energy distribution and composite narrowband IPL 500-600 nm energy distribution of 0.081μm radius vessel. Composite vessel indicates that most absorbed energy is contained within the top half of the vessel, while the bottom half has lower absorbed energy compared to 595 nm. C) Line profile of normalized absorbed energy distribution using 595nm and narrowband IPL irradiation. With the former, the average absorbed energy is more evenly distributed over the entire vessel, as compared to the narrowband IPL absorbed energy.

PDL			Narrowband IPL - Single			Narrowband IPL - Stacked		
Irradiance	Hem.	Shutdown	Irradiance	Hem.	Shutdown	Irradiance	Hem.	Shutdown
2167	yes	0	2800	yes	1	1250	yes	0
2167	yes	0	3000	no	0	1250	yes	0
2667	yes	0	3000	yes	0	1400	yes	0
2667	yes	0	3000	no	1	1400	yes	0
3667	yes	0	3000	yes	0	1600	yes	0
4000	yes	0	3000	yes	1	1750	yes	0
4000	yes	0	3333	no	0	1750	yes	0
4333	yes	0	3333	no	0	2000	yes	1
4333	yes	0	3333	no	0	2200	yes	0
4667	yes	1	3333	yes	0	2200	yes	0
4667	yes	0	3333	yes	1	2400	yes	1
5000	yes	0	4000	yes	0	2500	yes	0
5000	yes	0	4000	yes	0	2750	yes	1
5333	yes	1				2750	yes	0
5333	yes	1				2750	yes	1
5333	yes	1				2800	yes	1
6667	yes	1				3000	yes	1
6667	yes	1				3000	yes	0
						3000	yes	0
						3333	yes	1
						3333	yes	0
						3333	yes	0
						3333	yes	1
						3667	yes	1
						3667	no	0
						3667	yes	1
						4000	no	0

Table 2 Summary of observations of persistent vascular shutdown for experiments in which the PDL irradiance was 2167-5000 W/cm^2, the narrowband IPL single pulse irradiance was 2800-4000 kW/cm^2, and the narrowband IPL stacked pulse irradiance was 1250-2500 kW/cm^2. The data also displays the shutdown response for each experiment at its corresponding irradiance, showing the relationship between increasing irradiance and persistent vascular shutdown. Hemorrhage formation was observed in all experiments in which persistent vascular shutdown occurred, but not all experiments in which hemorrhage formation occurred resulted in shutdown. A binary scale of "0" (no persistent vascular shutdown on Day 7) or "1" (persistent vascular shutdown achieved on Day 7) was assigned to each image.

6.4 Discussion

Currently, the PDL is the gold standard technique in the treatment of PWS in the United States. On average, most patients typically require more than 15 sessions to achieve

either a lightening of the PWS or complete removal[75]. Many groups[101-103, 105, 112] have studied the use of IPL as an alternate method to treat PWS birthmarks. Previous results have demonstrated limited efficacy due to a large variation of parameters including pulse width, output energy, and spectral output. Here, we studied the effects of these parameters for photothermal therapy using narrowband IPL and compared it with data from PDL experiments.

We previously characterized PDL irradiation in order to determine the radiant exposures necessary to achieve persistent vascular shutdown[94]. Utilizing similar methods described in previously published studies to photocoagulate the vasculature[69, 70, 85], we employed dose response analysis to determine the characteristic radiant exposure (7.1 J/cm^2) required to induce persistent vascular shutdown using 595-nm PDL irradiation.

Here, we characterized the narrowband IPL in single and double (stacked) pulse configurations. To more directly compare the results of PDL and narrowband IPL irradiation, we used irradiance values instead of radiant exposure. We found that the irradiance values associated with persistent vascular shutdown for both PDL and narrowband IPL irradiation were in the same general range (Table 6.2). For PDL irradiation, irradiance values greater than 4667 kW/cm^2 were required to induce persistent vascular shutdown. For single pulse narrowband IPL, persistent vascular shutdown was induced with irradiances as low as 2800 kW/cm^2 and as high as 3333 kW/cm^2, but not in a consistent manner. Similarly, for double pulse narrowband IPL irradiation, persistent vascular shutdown was observed at irradiances from 2000-3667 kW/cm^2, but a clear trend between increasing irradiance and occurrence of persistent

vascular shutdown was not evident. Furthermore, with narrowband IPL irradiation, we were unable to identify a characteristic radiant exposure or irradiance required to achieve persistent vascular shutdown. Collectively, the data suggest that narrowband IPL irradiation with the parameters available in this specific IPL device, may cause persistent vascular shutdown at lower irradiances than the PDL, but in an inconsistent fashion.

Using double-pulse narrowband IPL irradiation, our data do not demonstrate a clear relationship between increasing irradiance and persistent vascular shutdown. This observation is consistent with other studies[105, 113, 114] in which a similar effect was observed of improved treatment outcome with an increasing number of pulses. One key difference between these studies and our present study is that they involved use of multiple treatment sessions of multiple pulses, compared to our single use of double pulse narrowband IPL. Further study of this narrowband IPL device is warranted to test the hypothesis that multiple treatments involving multiple light pulses correlate to improved treatment outcome.

To understand better the observed difference between narrowband IPL and PDL irradiation, we performed Monte Carlo computational simulations to estimate the optical energy deposition in subdermal blood vessels. This required analysis of the output spectrum of the narrowband IPL for two purposes: 1) to quantify the wavelength dependent contributions towards the total absorbed energy in our Monte Carlo simulations and 2) to calculate a weighted absorption coefficient at each wavelength along the spectrum. The weighted absorption coefficient was calculated by multiplying the oxyhemoglobin absorption spectrum by the relative intensity of the narrowband IPL output spectrum. Over the range of 500 to 600 nm, we calculated a value of 149 cm^{-1},

which is nearly four times higher than the absorption coefficient (35 cm^{-1}) at 595 nm. A higher oxyhemoglobin absorption coefficient suggests that for a given irradiance, the narrowband IPL treatment should result in increased rate of energy deposition than PDL treatment. While simultaneously analyzing the weighted absorption coefficient, we compared experimentally observed treatment outcome results to those predicted by Monte Carlo computational simulation. Figure 6.2A shows the absorbed energy deposition on an average sized vessel (162 μm diameter) found in the dorsal window chamber model. While the modeling was performed using a simplified simulated geometry (i.e., the vessel in the window chamber is represented by a cylinder and each tissue layer has homogeneous absorption and scattering coefficients throughout its depth), we estimated the localized energy deposition within the vessel at different wavelengths. From 500 to 585 nm, the model predicts an energy deposition 53.2% higher at the top half of the vessel compared to the bottom half. At 595 and 600 nm, the total absorbed energy distribution is much more uniform, which can lead to more efficient conversion of light to heat.

Figure 6.2B shows the comparison between the combined total absorbed energy over all wavelengths, weighted by the intensity spectrum of the narrowband IPL. On the left side of Figure 6.2B, we see the total absorbed energy plot at only 595 nm. Due to the nature of the uniform and even energy distribution of the 595 nm, the PDL may be more effective in causing blood flow shutdown in the vessel because the temperature of the entire vessel is allowed to rise to a value associated with permanent damage[74]. This effect was demonstrated by Heger et al[74], who observed that inhomogeneous photon distribution and subsequent subcritical temperature increase could be a source of incomplete photocoagulation within vessels, leading to a suboptimal treatment outcome.

Figure 6.2C shows a line profile of the normalized total energy absorption profile at 595 nm compared with combined total absorbed energy of the narrowband IPL. While the combined total absorbed energy of the IPL is higher in the top half of the vessel energy, we see an intersection point roughly half way into the vessel. Thus, as we move deeper into the combined total absorbed energy distribution, the absorbed energy drops off much more quickly compared to the 595 nm absorbed energy, which indicates that less energy is absorbed deeper into the vessel in narrowband IPL treatments compared to the PDL.

Collectively, based on our preclinical data (Table 6.2) and modeling data (Figure 6.2), we believe that further study is warranted to refine the narrowband IPL technology to treat PWS birthmarks. Future investigations of this device would include both longer and shorter pulse durations, increasing radiant exposures, and additional pulses beyond the single/double pulse protocol. The prevailing thought behind IPL usage to treat PWS birthmarks is that by using a broad range of wavelengths, absorption of the light during photothermolysis can be enhanced by absorption over the entire hemoglobin spectra. By calculating the weighted absorption coefficient at each wavelength, we can model the effects of broadband irradiation to study the full interactions between light dosimetry and treatment outcome. Additionally, the narrowband IPL can be further tuned to optimize a specific wavelength range that can be used to treat PWS, whereas the PDL only operates at discrete wavelengths.

6.5 Acknowledgements

The work was supported in part by grants obtained from the National Institutes of Health (R01HD065536), the National Institutes of Health Laser Microbeam and Medical Program (P41EB015890 and NIH K25-EB007309), the Arnold and Mabel Beckman

Foundation, and the University of California, Irvine Undergraduate Research Opportunities Program. The authors thank Alma Lasers for their generosity in providing us with the IPL device. The authors would also like to acknowledge Dr. Austin Moy (The University of Texas at Austin) for guidance and assistance with preparation of this manuscript.

Chapter 7 - SUMMARY AND CONCLUDING REMARKS

The current gold standard treatment for PWS birthmarks in the US is the use of the pulsed dye laser, which has significant limitations. Many patients undergo 15 or more laser treatments without clearance of the port wine stain[13, 14]. Alternatives to PDL treatment include photodynamic therapy, combined PDT/PDL protocols, and other light based treatments, all of which have the potential to overcome the shortcomings of current treatments and achieve complete and consistent port wine stain clearance.

Photodynamic therapy has demonstrated promise towards achieving a better treatment outcome for PWS birthmarks, however, careful selection of treatment parameters is needed in order to avoid deep vascular damage leading to skin necrosis. To this end, we focused on characterizing two photosensitizers, NPe6 and Hemoporfin, to better develop safe treatment parameters. We performed PDT studies using the rodent dorsal window chamber model, an in vivo model of the skin microvasculature. During the course of these studies, we monitored skin blood flow dynamics using laser speckle imaging, studied the photosensitizer pharmacokinetics with intravital microscopy, and performed dose response analysis to determine the characteristic radiant exposures for each drug/light combination.

We then investigated a combined PDT/PDL protocol, where the light dosage of PDT and PDL were selected within the safe radiant exposure regime of each therapy. We determined that a synergistic effect exists between the PDT and PDL protocols, illustrating that this combined approach leads to a desired treatment outcome while minimizing risk of epidermal damage (PDL) and deep vascular damage (PDT). This further reduces the probability that poor treatment outcomes like scarring and skin necrosis will occur.

Our research efforts then turned to characterizing and quantifying the depth of injury caused by NPe6-mediated PDT. This study was performed on rat skin, a much different model compared to the mouse model with respect to morphology, size, and density of blood vessels. Our research has demonstrated that NPe6-mediated PDT causes specific, targeted vascular damage initially, which then leads to ischemic necrosis as the shutdown blood vessels are no longer able to deliver oxygen and nutrients to the surrounding tissue. Caspase 3 staining at 9 hours clearly demonstrated the vascular specific nature of the treatment, as apoptosis was clearly seen in the endothelial cells lining the blood vessels affected by treatment. We also confirmed the direct, but non-linear relationship between depth of ischemic changes and light dose administered.

In our investigation of alternative light based approaches, we focused on the Alma Dye-VL Intense Pulsed Light (IPL), and performed a direct comparison study to the PDL. We used Monte Carlo computational simulations to determine that the absorbed light distribution is not uniform when using multiple wavelengths (500-600 nm) for irradiation, compared to a more even distribution in the 595 nm PDL. Absorption of light energy at the top of the vessel may cause a higher temperature increase, resulting an uneven temperature distribution that may lead to be a better treatment outcome. It was also observed that the IPL could deliver lower radiant exposures over longer pulse durations in order to achieve vascular shutdown in the mouse model, compared to the PDL.

Future work includes translating the treatment parameters investigated in these preclinical studies into the clinic and an initial pilot study to determine the clinical efficacy of these treatment parameters has already been initiated. We have successfully demonstrated NPe6-mediated PDT and a combined treatment protocol of NPe6-mediated

PDT and the PDL as a proof of concept. Further investigation of NPe6-mediated PDT mechanisms is crucial to determining effective treatment parameters. Proposed experiments include performing the combined PDT/PDL protocol on the rat model and using immunohistochemistry stains like Caspase 3, and Smooth Muscle Actin (SMA) to identify blood vessels that have undergone apoptosis as a result of photothermal and photochemical treatment. Characterizing PDL treatment on the rat model may also be of interest to better understand the mechanism of injury and to optimize treatment parameters when combined with PDT. Finally, exploration into other currently used photosensitizers, such as Foscan, Tookad, or other new generation photosensitizers may be of interest to combination therapy with the PDL, which may improve treatment outcomes.

References

1. Habif, T.P., et al., *Skin Disease: Diagnosis and Treatment, 3e*. 3 edition ed. 2011, Edinburgh: Saunders. 692.
2. Jacobs, A.H. and R.G. Walton, *The incidence of birthmarks in the neonate.* Pediatrics, 1976. **58**(2): p. 218-222.
3. Tallman, B., et al., *Location of port-wine stains and the likelihood of ophthalmic and/or central nervous system complications.* Pediatrics, 1991. **87**(3): p. 323-327.
4. Smoller, B.R., *Lever's Histopathology of the Skin, 10th edition.* Journal of Cutaneous Pathology, 2009. **36**(5): p. 605-605.
5. Heller, A., et al., *Birth defects and psychosocial adjustment.* American Journal of Diseases of Children (1960), 1985. **139**(3): p. 257-263.
6. Nelson, J.S., *Selective photothermolysis and removal of cutaneous vasculopathies and tattoos by pulsed laser.* Plastic and Reconstructive Surgery, 1991. **88**(4): p. 723-731.
7. Ashinoff, R. and R.G. Geronemus, *Flashlamp-pumped pulsed dye laser for port-wine stains in infancy: earlier versus later treatment.* Journal of the American Academy of Dermatology, 1991. **24**(3): p. 467-472.
8. Kelly, K.M. and J.S. Nelson, *Update on the Clinical Management of Port Wine Stains.* Lasers in Medical Science, 2000. **15**(4): p. 220-226.
9. Chapas, A.M., K. Eickhorst, and R.G. Geronemus, *Efficacy of early treatment of facial port wine stains in newborns: a review of 49 cases.* Lasers in Surgery and Medicine, 2007. **39**(7): p. 563-568.
10. Lanigan, S.W., *Port-wine stains unresponsive to pulsed dye laser: explanations and solutions.* The British Journal of Dermatology, 1998. **139**(2): p. 173-177.
11. van der Horst, C.M., et al., *Effect of the timing of treatment of port-wine stains with the flash-lamp-pumped pulsed-dye laser.* The New England Journal of Medicine, 1998. **338**(15): p. 1028-1033.
12. Yohn, J.J., et al., *Lesion size is a factor for determining the rate of port-wine stain clearing following pulsed dye laser treatment in adults.* Cutis, 1997. **59**(5): p. 267-270.
13. Milanič, M., et al., *Numerical optimization of sequential cryogen spray cooling and laser irradiation for improved therapy of port wine stain.* Lasers in Surgery and Medicine, 2011. **43**(2): p. 164-175.
14. Yuan, K.-H., et al., *Comparison of photodynamic therapy and pulsed dye laser in patients with port wine stain birthmarks: a retrospective analysis.* Photodiagnosis and Photodynamic Therapy, 2008. **5**(1): p. 50-57.
15. Babilas, P., et al., *Selective photothermolysis of blood vessels following flashlamp-pumped pulsed dye laser irradiation: in vivo results and mathematical modelling are in agreement.* The Journal of Investigative Dermatology, 2005. **125**(2): p. 343-352.
16. Edström, D.W., M.A. Hedblad, and A.M. Ros, *Flashlamp pulsed dye laser and argon-pumped dye laser in the treatment of port-wine stains: a clinical and histological comparison.* The British Journal of Dermatology, 2002. **146**(2): p. 285-289.
17. L. T. Norvang, E.J.F., *Epidermal melanin absorption in human skin.* Proceedings of SPIE - The International Society for Optical Engineering, 1995. **2624**: p. 143-154.

18. van Gemert, M.J., et al., *Non-invasive determination of port wine stain anatomy and physiology for optimal laser treatment strategies.* Physics in Medicine and Biology, 1997. **42**(5): p. 937-950.
19. Kalka, K., H. Merk, and H. Mukhtar, *Photodynamic therapy in dermatology.* Journal of the American Academy of Dermatology, 2000. **42**(3): p. 389-413.
20. Dougherty, T.J., et al., *Photodynamic Therapy.* Journal of the National Cancer Institute, 1998. **90**(12): p. 889-905.
21. Weishaupt, K.R., C.J. Gomer, and T.J. Dougherty, *Identification of singlet oxygen as the cytotoxic agent in photoinactivation of a murine tumor.* Cancer Research, 1976. **36**(7 PT 1): p. 2326-2329.
22. Raabe, O., *Ueber die Wirkung fluoreszierende Stoffe auf infusorien.* Zeitschrift fuer Biologie, 1900. **39**: p. 524-526.
23. Meyer-Betz, F., *Untersuchungen ¨uber die biologische (photodynamische) Wirkung des H¨amatoporphyrins und andere Derivate des Blutund Gallenfarbstoffs.* Dtsch. Arch. Klin. Med., 1913. **112**: p. 450-476.
24. Dougherty, T.J., et al., *Photoradiation therapy for the treatment of malignant tumors.* Cancer Research, 1978. **38**(8): p. 2628-2635.
25. Lipson, R.L. and E.J. Baldes, *The photodynamic properties of a particular hematoporphyrin derivative.* Archives of Dermatology, 1960. **82**: p. 508-516.
26. Lipson, R.L., E.J. Baldes, and A.M. Olsen, *The use of a derivative of hematoporhyrin in tumor detection.* Journal of the National Cancer Institute, 1961. **26**: p. 1-11.
27. Ochsner, M., *Photophysical and photobiological processes in the photodynamic therapy of tumours.* Journal of Photochemistry and Photobiology. B, Biology, 1997. **39**(1): p. 1-18.
28. Kroemer, G., B. Dallaporta, and M. Resche-Rigon, *The mitochondrial death/life regulator in apoptosis and necrosis.* Annual Review of Physiology, 1998. **60**: p. 619-642.
29. Lilge, L., M. Portnoy, and B.C. Wilson, *Apoptosis induced in vivo by photodynamic therapy in normal brain and intracranial tumour tissue.* British Journal of Cancer, 2000. **83**(8): p. 1110-1117.
30. Oleinick, N.L., R.L. Morris, and I. Belichenko, *The role of apoptosis in response to photodynamic therapy: what, where, why, and how.* Photochemical & Photobiological Sciences: Official Journal of the European Photochemistry Association and the European Society for Photobiology, 2002. **1**(1): p. 1-21.
31. Henderson, B.W. and V.H. Fingar, *Oxygen limitation of direct tumor cell kill during photodynamic treatment of a murine tumor model.* Photochemistry and Photobiology, 1989. **49**(3): p. 299-304.
32. Busch, T.M., et al., *Photodynamic therapy creates fluence rate-dependent gradients in the intratumoral spatial distribution of oxygen.* Cancer Research, 2002. **62**(24): p. 7273-7279.
33. Fuchs, J. and J. Thiele, *The role of oxygen in cutaneous photodynamic therapy.* Free Radical Biology & Medicine, 1998. **24**(5): p. 835-847.
34. Tromberg, B.J., et al., *Tumor oxygen tension during photodynamic therapy.* Journal of Photochemistry and Photobiology. B, Biology, 1990. **5**(1): p. 121-126.

35. Tromberg, B.J., et al., *In vivo tumor oxygen tension measurements for the evaluation of the efficiency of photodynamic therapy.* Photochemistry and Photobiology, 1990. **52**(2): p. 375-385.
36. Lin, G.C., et al., *Skin necrosis due to photodynamic action of benzoporphyrin depends on circulating rather than tissue drug levels: implications for control of photodynamic therapy.* Photochemistry and Photobiology, 1998. **68**(4): p. 575-583.
37. Kelly, K.M., et al., *Combined photodynamic and photothermal induced injury enhances damage to in vivo model blood vessels.* Lasers in Surgery and Medicine, 2004. **34**(5): p. 407-413.
38. Kimel, S., et al., *Synergistic photodynamic and photothermal treatment of port-wine stain?* Lasers in Surgery and Medicine, 2004. **34**(2): p. 80-82.
39. Smith, T.K., et al., *Microvascular blood flow dynamics associated with photodynamic therapy, pulsed dye laser irradiation and combined regimens.* Lasers in Surgery and Medicine, 2006. **38**(5): p. 532-539.
40. Channual, J., et al., *Vascular effects of photodynamic and pulsed dye laser therapy protocols.* Lasers in Surgery and Medicine, 2008. **40**(9): p. 644-650.
41. Tournas, J.A., et al., *Combined benzoporphyrin derivative monoacid ring photodynamic therapy and pulsed dye laser for port wine stain birthmarks.* Photodiagnosis and Photodynamic Therapy, 2009. **6**(3-4): p. 195-199.
42. Gu, Y., et al., *[Clinical study of 1949 cases of port wine stains treated with vascular photodynamic therapy (Gu's PDT)].* Annales De Dermatologie Et De Vénéréologie, 2007. **134**(3 Pt 1): p. 241-244.
43. Lu, Y.-G., et al., *Photodynamic therapy of port-wine stains.* The Journal of Dermatological Treatment, 2010. **21**(4): p. 240-244.
44. Yu, W., et al., *18 years long-term results of facial port-wine stain (PWS) after photodynamic therapy (PDT)--a case report.* Photodiagnosis and Photodynamic Therapy, 2015. **12**(1): p. 143-145.
45. Yuan, K.-H., J.-H. Gao, and Z. Huang, *Adverse effects associated with photodynamic therapy (PDT) of port-wine stain (PWS) birthmarks.* Photodiagnosis and Photodynamic Therapy, 2012. **9**(4): p. 332-336.
46. Zhao, Y., et al., *Efficacy and safety of hemoporfin in photodynamic therapy for port-wine stain: a multicenter and open-labeled phase IIa study.* Photodermatology, Photoimmunology & Photomedicine, 2011. **27**(1): p. 17-23.
47. Qin, Z.-P., et al., *Photodynamic therapy of port wine stains-a report of 238 cases.* Photodiagnosis and Photodynamic Therapy, 2007. **4**(1): p. 53-59.
48. Moy, A.J., et al., *Wide-field functional imaging of blood flow and hemoglobin oxygen saturation in the rodent dorsal window chamber.* Microvascular Research, 2011. **82**(3): p. 199-209.
49. Papenfuss, H.D., et al., *A transparent access chamber for the rat dorsal skin fold.* Microvascular Research, 1979. **18**(3): p. 311-318.
50. Briers, J.D. and A.F. Fercher, *Retinal blood-flow visualization by means of laser speckle photography.* Investigative Ophthalmology & Visual Science, 1982. **22**(2): p. 255-259.
51. Fercher, A.F. and J.D. Briers, *Flow visualization by means of single-exposure speckle photography.* Optics Communications, 1981. **37**(5): p. 326-330.
52. Cheng, H. and T.Q. Duong, *Simplified laser-speckle-imaging analysis method and its application to retinal blood flow imaging.* Optics Letters, 2007. **32**(15): p. 2188-2190.

53. Ramirez-San-Juan, J.C., et al., *Impact of velocity distribution assumption on simplified laser speckle imaging equation.* Optics Express, 2008. **16**(5): p. 3197-3203.
54. Goodman, J.W., *Statistical properties of laser speckle patterns*, in *Laser Speckle and Related Phenomena*. 1975, Springer Berlin Heidelberg. p. 9-75.
55. Briers, J.D., *Laser Doppler and time-varying speckle: a reconciliation.* Journal of the Optical Society of America A, 1996. **13**(2).
56. Ridler, T. and S. Calvard, *Picture Thresholding Using an Iterative Selection Method.* Systems, Man and Cybernetics, IEEE Transactions on, 1978. **8**(8): p. 630-632.
57. Barton, J.K., et al., *Simultaneous irradiation and imaging of blood vessels during pulsed laser delivery.* Lasers in Surgery and Medicine, 1999. **24**(3): p. 236-243.
58. Chan, A.L., et al., *Pharmacokinetics and clinical effects of mono-L-aspartyl chlorin e6 (NPe6) photodynamic therapy in adult patients with primary or secondary cancer of the skin and mucosal surfaces.* Photodermatology, Photoimmunology & Photomedicine, 2005. **21**(2): p. 72-78.
59. Kimel, S., et al., *Influence of laser wavelength and pulse duration on gas bubble formation in blood filled glass capillaries.* Lasers in Surgery and Medicine, 2005. **36**(4): p. 281-288.
60. Chan, K.F., et al., *Free electron laser lithotripsy: threshold radiant exposures.* Journal of Endourology / Endourological Society, 2000. **14**(2): p. 161-167.
61. Vallee, J., et al., *Lasers in the treatment of vascular lesions.* In: Kaminer MS, Arndt KA, Dover JS, Rohrer TE, Zachary CB, editors. Atlas of cosmetic surgery., 2009.
62. Mitra, S. and T.H. Foster, *In vivo confocal fluorescence imaging of the intratumor distribution of the photosensitizer mono-L-aspartylchlorin-e6.* Neoplasia (New York, N.Y.), 2008. **10**(5): p. 429-438.
63. Fingar, V.H., et al., *The role of microvascular damage in photodynamic therapy: the effect of treatment on vessel constriction, permeability, and leukocyte adhesion.* Cancer Research, 1992. **52**(18): p. 4914-4921.
64. McMahon, K.S., et al., *Effects of photodynamic therapy using mono-L-aspartyl chlorin e6 on vessel constriction, vessel leakage, and tumor response.* Cancer Research, 1994. **54**(20): p. 5374-5379.
65. Bui, A.K., et al., *Longitudinal, multimodal functional imaging of microvascular response to photothermal therapy.* Optics Letters, 2010. **35**(19): p. 3216-3218.
66. Choi, B., et al., *The importance of long-term monitoring to evaluate the microvascular response to light-based therapies.* The Journal of Investigative Dermatology, 2008. **128**(2): p. 485-488.
67. Choi, B., N.M. Kang, and J.S. Nelson, *Laser speckle imaging for monitoring blood flow dynamics in the in vivo rodent dorsal skin fold model.* Microvascular Research, 2004. **68**(2): p. 143-146.
68. Choi, B., et al., *Linear response range characterization and in vivo application of laser speckle imaging of blood flow dynamics.* Journal of Biomedical Optics, 2006. **11**(4).
69. Barton, J.K., et al., *Laser fluence for permanent damage of cutaneous blood vessels.* Photochemistry and Photobiology, 1999. **70**(6): p. 916-920.
70. Vargas, G., J.K. Barton, and A.J. Welch, *Use of hyperosmotic chemical agent to improve the laser treatment of cutaneous vascular lesions.* Journal of Biomedical Optics, 2008. **13**(2).

71. Usuda, J., et al., *Photodynamic therapy for lung cancers based on novel photodynamic diagnosis using talaporfin sodium (NPe6) and autofluorescence bronchoscopy.* Lung Cancer (Amsterdam, Netherlands), 2007. **58**(3): p. 317-323.
72. Gomer, C.J. and A. Ferrario, *Tissue distribution and photosensitizing properties of mono-L-aspartyl chlorin e6 in a mouse tumor model.* Cancer Research, 1990. **50**(13): p. 3985-3990.
73. Geronemus, R.G. and R. Ashinoff, *The medical necessity of evaluation and treatment of port-wine stains.* The Journal of Dermatologic Surgery and Oncology, 1991. **17**(1): p. 76-79.
74. Heger, M., et al., *Towards optimization of selective photothermolysis: prothrombotic pharmaceutical agents as potential adjuvants in laser treatment of port wine stains. A theoretical study.* Thrombosis and Haemostasis, 2005. **93**(2): p. 242-256.
75. Koster, P.H., et al., *Prediction of portwine stain clearance and required number of flashlamp pumped pulsed dye laser treatments.* Lasers in Surgery and Medicine, 2001. **29**(2): p. 151-155.
76. Kaiser, P.K., et al., *Verteporfin plus ranibizumab for choroidal neovascularization in age-related macular degeneration: twelve-month results of the DENALI study.* Ophthalmology, 2012. **119**(5): p. 1001-1010.
77. Houle, J.-M. and H.A. Strong, *Duration of skin photosensitivity and incidence of photosensitivity reactions after administration of verteporfin.* Retina (Philadelphia, Pa.), 2002. **22**(6): p. 691-697.
78. Akimoto, J., J. Haraoka, and K. Aizawa, *Preliminary clinical report on safety and efficacy of photodynamic therapy using talaporfin sodium for malignant gliomas.* Photodiagnosis and Photodynamic Therapy, 2012. **9**(2): p. 91-99.
79. Ikeda, N., et al., *New aspects of photodynamic therapy for central type early stage lung cancer.* Lasers in Surgery and Medicine, 2011. **43**(7): p. 749-754.
80. Kujundzić, M., et al., *A Phase II safety and effect on time to tumor progression study of intratumoral light infusion technology using talaporfin sodium in patients with metastatic colorectal cancer.* Journal of Surgical Oncology, 2007. **96**(6): p. 518-524.
81. Lustig, R.A., et al., *A multicenter Phase I safety study of intratumoral photoactivation of talaporfin sodium in patients with refractory solid tumors.* Cancer, 2003. **98**(8): p. 1767-1771.
82. Yano, T., et al., *Phase I study of photodynamic therapy using talaporfin sodium and diode laser for local failure after chemoradiotherapy for esophageal cancer.* Radiation Oncology (London, England), 2012. **7**.
83. Bromley, E., et al., *Characterization of cutaneous photosensitivity in healthy volunteers receiving talaporfin sodium.* Photodermatology, Photoimmunology & Photomedicine, 2011. **27**(2): p. 85-89.
84. Ohshiro, T., et al., *Histological responses of cutaneous vascular lesions following photodynamic therapy with talaporfin sodium: a chicken comb model.* The Keio Journal of Medicine, 2009. **58**(3): p. 176-184.
85. Moy, W.J., et al., *Preclinical in vivo evaluation of NPe6-mediated photodynamic therapy on normal vasculature.* Lasers in Surgery and Medicine, 2012. **44**(2): p. 158-162.
86. Nugent, L.J. and R.K. Jain, *Plasma pharmacokinetics and interstitial diffusion of macromolecules in a capillary bed.* The American Journal of Physiology, 1984. **246**(1 Pt 2): p. H129-137.

87. Zhou, X., et al., *Analysis of effective molecular diffusion rates for verteporfin in subcutaneous versus orthotopic Dunning prostate tumors.* Photochemistry and Photobiology, 2004. **79**(4): p. 323-331.
88. Madsen, S.J., et al., *Effects of combined photodynamic therapy and ionizing radiation on human glioma spheroids.* Photochemistry and Photobiology, 2002. **76**(4): p. 411-416.
89. Barton, J.K., et al., *Cooperative phenomena in two-pulse, two-color laser photocoagulation of cutaneous blood vessels.* Photochemistry and Photobiology, 2001. **73**(6): p. 642-650.
90. Svaasand, L.O., et al., *Increase of dermal blood volume fraction reduces the threshold for laser-induced purpura: implications for port wine stain laser treatment.* Lasers in Surgery and Medicine, 2004. **34**(2): p. 182-188.
91. Gorman, S.A., S.B. Brown, and J. Griffiths, *An overview of synthetic approaches to porphyrin, phthalocyanine, and phenothiazine photosensitizers for photodynamic therapy.* Journal of Environmental Pathology, Toxicology and Oncology: Official Organ of the International Society for Environmental Toxicology and Cancer, 2006. **25**(1-2): p. 79-108.
92. Pu, Y., W. Chen, and Z. Yu, *Research progress of Hemoporfin – Part one: Preclinical study.* Photodiagnosis and Photodynamic Therapy, 2012. **9**(2): p. 180-185.
93. Xiao, Q., et al., *Photodynamic therapy of port-wine stains: Long-term efficacy and complication in Chinese patients: Photodynamic therapy of port-wine stains.* The Journal of Dermatology, 2011. **38**(12): p. 1146-1152.
94. Kelly, K.M., et al., *Talaporfin sodium-mediated photodynamic therapy alone and in combination with pulsed dye laser on cutaneous vasculature.* The Journal of Investigative Dermatology, 2015. **135**(1): p. 302-304.
95. Zhou, G.Y. and Z.Y. Zhang, *[Preliminary clinical study on krypton laser photodynamic therapy for PWS].* Shanghai Kou Qiang Yi Xue = Shanghai Journal of Stomatology, 2000. **9**(3): p. 168-170.
96. Astner, S. and R.R. Anderson, *Treating vascular lesions.* Dermatologic Therapy, 2005. **18**(3): p. 267-281.
97. Mulligan, P.R., et al., *Vascular anomalies: classification, imaging characteristics and implications for interventional radiology treatment approaches.* The British Journal of Radiology, 2014. **87**(1035).
98. Chen, D., et al., *Nodules arising within port-wine stains: a clinicopathologic study of 31 cases.* The American Journal of Dermatopathology, 2011. **33**(2): p. 144-151.
99. Waldorf, H.A., et al., *Effect of dynamic cooling on 585-nm pulsed dye laser treatment of port-wine stain birthmarks.* Dermatologic Surgery: Official Publication for American Society for Dermatologic Surgery [et Al.], 1997. **23**(8): p. 657-662.
100. Anderson, R.R. and J.A. Parrish, *Selective photothermolysis: precise microsurgery by selective absorption of pulsed radiation.* Science, 1983. **220**(4596): p. 524-7.
101. Bjerring, P., K. Christiansen, and A. Troilius, *Intense pulsed light source for the treatment of dye laser resistant port-wine stains.* Journal of Cosmetic and Laser Therapy: Official Publication of the European Society for Laser Dermatology, 2003. **5**(1): p. 7-13.
102. Dong, X., et al., *Treatment of facial port-wine stains with a new intense pulsed light source in Chinese patients.* Journal of Cosmetic and Laser Therapy: Official Publication of the European Society for Laser Dermatology, 2010. **12**(4): p. 183-187.

103. Babilas, P., et al., *Split-face comparison of intense pulsed light with short- and long-pulsed dye lasers for the treatment of port-wine stains.* Lasers Surg Med, 2010. **42**(8): p. 720-7.
104. Adatto, M.A., J. Luc-Levy, and S. Mordon, *Efficacy of a novel intense pulsed light system for the treatment of port wine stains.* Journal of Cosmetic and Laser Therapy: Official Publication of the European Society for Laser Dermatology, 2010. **12**(2): p. 54-60.
105. Li, G., et al., *Clinical analysis of port wine stains treated by intense pulsed light.* Journal of Cosmetic and Laser Therapy: Official Publication of the European Society for Laser Dermatology, 2010. **12**(1): p. 2-6.
106. Klein, A., et al., *Laser and IPL treatment of port-wine stains: therapy options, limitations, and practical aspects.* Lasers in Medical Science, 2011. **26**(6): p. 845-859.
107. Hale, G.M. and M.R. Querry, *Optical Constants of Water in the 200-nm to 200-microm Wavelength Region.* Applied Optics, 1973. **12**(3): p. 555-563.
108. Jacques, S.L., *Optical properties of biological tissues: a review.* Physics in Medicine and Biology, 2013. **58**(11): p. R37-61.
109. van Veen, R.L.P., et al., *Determination of visible near-IR absorption coefficients of mammalian fat using time- and spatially resolved diffuse reflectance and transmission spectroscopy.* Journal of Biomedical Optics, 2005. **10**(5).
110. Hayakawa, C.K., J. Spanier, and V. Venugopalan, *Comparative analysis of discrete and continuous absorption weighting estimators used in Monte Carlo simulations of radiative transport in turbid media.* Journal of the Optical Society of America. A, Optics, Image Science, and Vision, 2014. **31**(2): p. 301-311.
111. Wang, L., S.L. Jacques, and L. Zheng, *MCML--Monte Carlo modeling of light transport in multi-layered tissues.* Computer Methods and Programs in Biomedicine, 1995. **47**(2): p. 131-146.
112. Reynolds, N., et al., *The role of the Lumina intense pulsed light system in the treatment of port wine stains--a case controlled study.* British Journal of Plastic Surgery, 2005. **58**(7): p. 968-980.
113. Kuzmina, I., et al., *Contact and contactless diffuse reflectance spectroscopy: potential for recovery monitoring of vascular lesions after intense pulsed light treatment.* Journal of Biomedical Optics, 2011. **16**(4).
114. Wang, B., et al., *Treatment of neck port-wine stain with intense pulsed light in Chinese population.* Journal of Cosmetic and Laser Therapy: Official Publication of the European Society for Laser Dermatology, 2013. **15**(2): p. 85-90.